UNIVERSIDAD DE CHILE
FACULTAD DE CIENCIAS FÍSICAS Y MATEMÁTICAS
DEPARTAMENTO DE FÍSICA

ATOMIC SCALE STUDY OF MECHANICAL SPECTROSCOPY IN FCC METALS

TESIS PARA OPTAR AL GRADO DE MAGÍSTER EN CIENCIAS, MENCIÓN FÍSICA

MAURICIO ENRIQUE MORALES SOLER

PROFESOR GUÍA:
FERNANDO LUND PLANTAT

PROFESOR CO-GUÍA:
ALFREDO CARO

MIEMBROS DE LA COMISIÓN:
GONZALO GUTIÉRREZ GALLARDO
AQUILES SEPÚLVEDA OSSES
RODRIGO SOTO BERTRAN

SANTIAGO DE CHILE
2016

RESUMEN DE LA MEMORIA PARA OPTAR
AL TÍTULO DE MAGÍSTER EN CIENCIAS, MENCIÓN FÍSICA
POR: MAURICIO ENRIQUE MORALES SOLER
FECHA: 2016
PROF. GUÍA: SR. FERNANDO LUND PLANTAT
PROF. CO-GUÍA: SR ALFREDO CARO

ESTUDIO A ESCALA ATÓMICA DE ESPECTROSCOPÍA MECÁNICA EN METALES FCC

La fricción interna corresponde a la capacidad de los materiales de disipar la energía de ondas de sonido. Esta capacidad depende del tipo de material así como del tipo y cantidad de defectos que contenga. Durante muchos años se ha utilizado la espectrocopía mecánica para obtener información del material a través de distintos experimentos, midiendo por ejemplo la fricción interna de un material específico.

A pesar de la capacidad para medir fricción interna, hasta ahora es difícil conocer con precisión cuales son los mecanismos microscópicos que dan origen a la disipación de energía al interior del material. De particular interés es un pico en la curva de disipación interna versus temperatura llamado pico de Bordoni. La evidencia sugiere que la generación de este pico se debe a propiedades de las dislocaciones. Modelos teóricos que usan mecánica del continuo permiten una descripción cualitativa, pero no cuantitativa, del efecto.

Hasta ahora se ha estudiado el pico de Bordoni desde el punto de vista experimental y desde la mecánica del contínuo. En este trabajo se propone estudiar este efecto desde las simulaciones atomísticas a través de dinámica molecular. Para ello se generó una muestra de cobre de 892 800 átomos con dos dislocaciones ancladas y se generaron ondas de corte en el material. Se midió la tensión generada en la muestra y se encontraron las curvas de tensión-deformación. Luego se estudió la disipación de energía generada por la interacción de las ondas con las dislocaciones a través de una posible histéresis en las curvas de tensión-deformación. Estas simulaciones se realizaron a las temperaturas de 0, 50, 100, 150, 200 y 250 K, con períodos de 125 ps y 38 ps y un máximo de deformación de 0.0008 y 0.008. Para estimar el orden de magnitud esperado para la respuesta del sistema se usó un modelo de cuerda sobreamortiguada, lo que también permitió estimar el período de forzamiento para el cual las pérdidas deberían ser máximas. Todo esto llevó a una estimación del cuociente entre energía disipada por ciclo y energía acumulada máxima llamado Q^{-1} del orden de 10^{-4} lo cual se ajusta a los resultados experimentales. Para estimar el valor de los parámetros que aparecen en el modelo analítico se realizaron simulaciones con las dislocaciones desancladas.

Dentro de la precisión numérica utilizada, no se encontró histéresis. Se deduce que la barrera de Peierls es muy pequeña para permitir detección de la histéresis. Se establece una cota para la precisión en las mediciones para cuantificar la fricción interna en el futuro.

Posibles direcciones de trabajo futuro incluyen la disminución de las fluctuaciones en las mediciones de la tensión, lo que se podría lograr con un mayor número de ciclos generados en las ondas de corte y promediando sobre muchas realizaciones. Otra opción es realizar las simulaciones en otros materiales, con mayores coeficientes de fricción, para aumentar la energía disipada.

ABSTRACT OF THESIS TO APPLY TO
THE TITLE OF MASTER IN SCIENCE, MAJOR IN PHYSICS
BY: MAURICIO ENRIQUE MORALES SOLER
DATE: 2016
THESIS ADVISOR: SR. FERNANDO LUND PLANTAT
THESIS CO-ADVISOR: SR ALFREDO CARO

ATOMIC SCALE STUDY OF MECHANICAL SPECTROSCOPY IN FCC METALS

Internal friction is the capacity of materials to dissipate the energy of sound waves inside of them. This capacity is dependant on the kind of material and also on the kind and amount of defects present. For many years a technique called mechanical spectroscopy has been used to obtain information of materials, measuring for example the internal friction.

Despite the capacity to measure internal friction, until now it has been hard to know with precision which are the microscopic origins of the dissipation of energy in different materials. Of particular interest is a peak in the curve of internal friction versus temperature called Bordoni peak. The evidence suggests that the generation of this peak is due to properties of dislocations. Theoretical models based on continuum mechanics permit a qualitative description, but not a quantitative one.

Until now the Bordoni peak has been studied from an experimental point of view and from a continuum mechanics approach. In this work it is proposed to study this effect from molecular dynamics simulations. For this, a copper sample with 892000 atoms and two anchored dislocations was generated. Shear waves were also generated in the sample. The average shear stress was measured and the stress-strain curves were found. Then, the dissipation of energy generated by the interactio between the dislocations and the shear waves was studied through the hysteresis in the stress-strain curves. These simulations were done at temperatures 0, 50, 100, 150, 200 y 250 K, with periods of 125 ps and 38 ps and a maximum of strain 0.0008 and 0.008. To estimate the order of magnitude expected in the simulations, a model of an overdamped string was used, which also permitted to estimate the period required to make the dissipation maximum. The estimated dissipated energy per cycle was 10^{-4} which is a similar result to reported experiments.

Within the numerical precision used, there was no hysteresis found. It is deduced that the Peierls barrier is too small to permit the detection of the hysteresis. A minimum of precision is established in the measurements to quantify the internal friction in the future.

Possible directions of future work include diminishing the of the fluctuations in the measurements of stress, which could be done by increasing the cycles and averaging over many realizations. Another option is to make simulations in other materials with greater friction coefficients, to increase the dissipated energy.

La ciencia siempre está equivocada, no puede resolver un problema sin crear diez más.
Fiódor Dostoyevski

Agradecimientos

Comienzo agradeciendo a mi familia, mis padres y mi hermano. A ellos agradezco acompañarme todo este tiempo, el apoyo, las risas e incluso las discusiones, gracias por absolutamente todo. De todo aquello aprendí mucho, los amo.

Agradecer también a todos mis amigos, de la vida, del colegio, de la universidad. Ojalá pudiera nombrarlos a todos, pero su compañía, ya sea en carretes, viajando, estudiando o simplemente tomándose unas chelas, no es algo que olvidaré. Gracias a los cabros wenlocos: Tomi, Siraquian, Rene, el waton, el mediano, Contesse, Munzer, Joaquin, Yair y más gente que me acompañaron desde el colegio y desde entonces hemos tenido que soportarnos en carretes, viajes, pichangas, etc. Gracias también por enseñarme el valor de la amistad. Gracias a los amigos de la U, al Matías por su gran amistad (y por convencerme de viajar a Brasil), al Joao, Fefo, Camilo, Diego, y muchísimos nombres que se me vienen a la mente de amigos de la universidad, lamentablemente no podría nombrarlos en esta hoja a todos ni agradecerles lo suficiente por hacer de mi paso por esta universidad una verdadera aventura de vida. Agradecer también a amigos que he conocido durante mi vida, en distintos mochileos y viajes, a la Fabiola por enseñarme la importancia del optimismo, me acuerdo de Chiloé donde conocí al Garo y el Rolo, gracias por recordarme lo importante de buscar la aventura. También mencionar a los cabros de la comisión de subcontrato, con quienes aprendí el valor de la lucha. Muchas gracias a todos mis amigos, por enseñarme a nunca perder el sentido de la aventura y el sentido del humor.

Agradecer finalmente a mis profesores guías, Fernando Lund y Alfredo Caro. Gracias por todo lo que me enseñaron durante este tiempo, por la oportunidad de poder trabajar con ellos y especialmente por enseñarme los valores de paciencia y trabajo duro que se requieren en la vida de un científico y en la vida en general.

Contents

Introduction **1**

1 Introduction to some concepts in Mechanical Spectroscopy **3**
1.1 Internal friction 3

2 Elasticity and anelasticity in solids **7**
2.1 Ideal Elasticity 7
2.2 Anelasticity 8
2.2.1 Anelastic relaxation 8
2.2.2 Anelastic dynamic response 9
2.2.3 Mechanical models of anelasticity 11
2.2.4 Origin of anelastic behaviour 14
2.2.5 Properties of the anelastic solid as function of temperature 15

3 Influence of lattice periodicity on dislocations **16**
3.1 Peierls-Nabarro dislocation model 16
3.1.1 Stress and displacement in the core 17
3.1.2 Elastic energy in Peierls Nabarro model 20
3.1.3 Criticism to Peierls Nabarro Model 23

4 The Bordoni peak **24**
4.1 Characteristics of the Bordoni Peak 25
4.2 Seeger's theory of the Bordoni Peak 25
4.2.1 Connection of Seeger's theory with experiment 29
4.3 Bordoni Peak and experiments 29

5 Molecular Dynamics simulation **30**
5.1 Preparation of samples 31
5.2 Finding hysteresis in Cu 32
5.3 Estimation of internal friction 35
5.3.1 Estimation of ΔW 35
5.3.2 Estimation of W 40
5.3.3 Estimation of $\tan\phi$ 42
5.3.4 Limitations of estimation 42
5.4 Simulation of internal friction 42
5.4.1 Limitations of simulation 45

Conclusion **49**

Bibliography **51**

Appendices **54**

A Time lengths for simulations **55**

B Partial dislocations in FCC metals **56**

Introduction

Mechanical spectroscopy is a technique used to study the mechanical properties of materials by the application of time dependent mechanical stresses on the sample and measuring the response generated by it. This technique has been used since the half of the last century, but the meaning of the measurements are still being debated in many cases [1].

One of these cases is the so called Bordoni peak. In 1946 Bordoni found that FCC metals subject to work hardening generated a peak in the internal friction versus temperature curve in the range of the 50 K to the 100 K. After the experimental characterization of this peak many speculations were made about the possible origin of this effect (see for example [2], [3]). But the specific microscopic processes involved are still unknown. Qualitatively, however, there is a strong evidence that points to dislocations as the origin for this effect [4].

Simulating the effect of dislocations on the internal friction of a metal is thus an interesting problem, which could shed light on the microscopic mechanism which generates the Bordoni peak. Understanding this mechanisms may give information on the defects in the materials, and thus on their mechanical properties [5], [6].

In this work we have performed numerical simulations of a FCC crystal system, more specifically copper, with dislocations in its interior, for the study of internal friction generation. The generation of internal friction in the sample was studied by applying oscillatory shear strains and measuring the resulting stress. The signature of internal friction is hysteresis in the stress-strain plot. The numerical simulations performed aimed at finding this hysteresis effect. To find the frequency at which the energy losses are maximum, an analytical model of the dislocation considered as an overdamped string was used. Once this frequency was found an oscillatory shear strain was applied at temperatures from 0 K to 250 K (range in which it would be expected to find the Bordoni peak). The area of the hysteresis loops was calculated and compared to the fluctuations of the measured stresses. The fluctuations of the measured stress were quantified, the size of the area produced by these fluctuations was found to be higher than the area of the expected hysteresis loop.

This thesis is organized as follows: chapter 1 reviews the concepts of elasticity and anelasticity in solids that provide a conceptual framework. Chapter 2 reviews current knowledge on the influence of lattice periodicity on dislocation dynamics. It is expected that this is a significant ingredient in the anelastic response of solids to dynamical loading. Chapter 3 reviews the data available on the Bordoni peak and the theoretical attempts at their comprehension. Chapter 4 describes the numerical simulations that have been performed in the search for hysteretic behaviour of the stress-strain curve of solids. This chapter is the main

original contribution of this thesis. A final chapter has concluding remarks. Some technical information about the simulations is gathered in the appendix.

Chapter 1

Introduction to some concepts in Mechanical Spectroscopy

In this chapter the technique of mechanical spectroscopy is introduced. The work of this thesis is to simulate through dynamical simulations a mechanical spectroscopy experiment. The objective of this chapter will be to introduce some concepts to understand the problem addressed in this thesis.

As mentioned in the introduction, mechanical spectroscopy is a technique used in material science to understand the mechanical properties in solids. In this technique, time dependent stresses are applied on the sample and the strain is measured (or viceversa). Generally in this measurements the temperature and the frequency of the time dependant stresses are varied to see how the mechanical properties vary with these quantities. An important property that can be measured is called the internal friction Q^{-1}, which quantifies the fraction of dissipated energy in a cycle. The mathematical definition in the context of a particular model (Maxwell-Voigt model) will be given in the next chapter and will be relevant for this thesis.

1.1 Internal friction

Internal friction is related to the dissipation of energy in a sample when mechanical stresses or strains are applied. Rather than give a precise mathematical definition in this section an account of the experiments to measure it will be given.

There are various techniques to measure internal friction, such as torsion pendulum or resonant ultrasound spectroscopy (RUS). To give some phenomenology of internal friction the torsion pendulum technique will be shown.

The torsion pendulum technique consists of taking a filament of a solid in which the internal friction will be measured and joining it to a pendulum at the bottom. An schematic image of this configuration is shown in figure 1.1. At an initial time, an amplitude θ_0 is given

to the pendulum, then the pendulum oscillates freely. The amplitude is then measured in time, an schematic graph that is obtained from this measurements is shown in figure 1.2. From the decay in the oscillation amplitude it is possible to calculate the internal friction by measuring how much the amplitude diminishes in a cycle. This can be done by calculating the coefficient of the exponential that fits the oscillation amplitudes.

If the amplitude of the oscillations is fitted by an exponential function as in figure 1.2, then this exponential will have the form

$$\theta(t) = \theta_0 \mathrm{e}^{-t\delta} \mathrm{e}^{\mathrm{i}\omega t}$$

where $\theta(t)$ and θ_0 are the amplitude at time t and at the initial time, δ is the decay coefficient and ω is the frequency of the oscillation. The decay coefficient can be related to the phase difference bewteen strain and stress ϕ by [4]

$$\delta = \pi\phi$$

This phase difference ϕ will be shown to be related to the internal friction Q^{-1} in the next chapter. The definition for internal friction is given in literature as [4]

$$Q^{-1} = \frac{\Delta W}{2\pi W}$$

where ΔW is the energy dissipated in each cycle and W is the maximum energy accumulated in the sample.

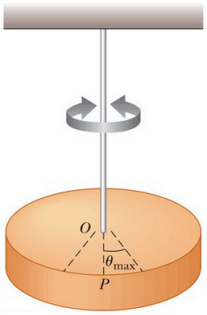

Figure 1.1: Torsion pendulum configuration. This configuration measures the internal friction in the filament shown in the figure.

An example of the measurements obtained are shown in 1.3. In the figure it is possible to see different measurements of internal friction Q^{-1} for different temperatures and different doses of neutron radiation (measured in dpa or displacements per atom). Through this measurements it is possible to deduce mechanical properties of the solid under study. The measurements of 1.3 were made on pure Fe, and in Fe-Cu alloys. Each of these samples were subject to different doses of neutron radiation, measured in dpa (displacements per atom) which measures the amount of radiation damage in neutron-irradiated materials, 1 dpa means for example that each atom in the material has been displaced from its site within the structural lattice of the material an average of 1 time. In the measurements it

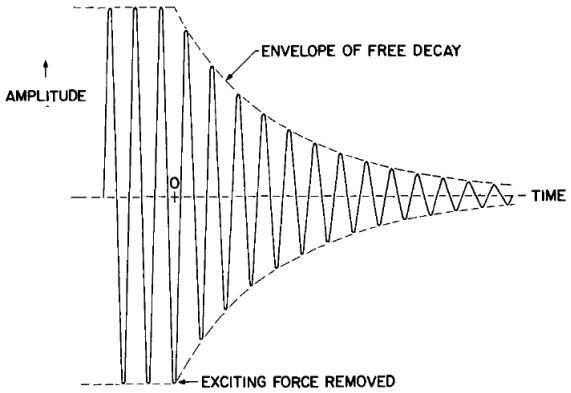

Figure 1.2: Amplitude of the oscillation in a torsion pendulum. From the decay in the amplitude it is possible to calculate the dissipation of energy in a cycle. Image modified from [4].

is observerd the appearance of several bumps in the internal friction curves as the radiation dose increases, this measurements can be related with mechanical properties such as the embrittlement of the material. In the article were these measurements are presented [5], only phenomenological explanations for the appearance of this bumps are given.

Through measurements of internal friction, several bumps in the internal friction can be identified. One particular bump is the Bordoni Peak, which appears in FCC metals. This peak is thought to be related to the inherent properties of dislocations, so measuring this peak can give valuable information about mechanical properties [4]. One such property is the Peierls barrier discussed in chapter 3. Although it is possible to determine this quantity through measurements of internal friction, this measurements seem to differ by at least 2 orders of magnitude from other experimental techniques such as mechanical deformation tests.

The difference in the measurement of the Peierls barrier has its source in the difficulty to interpret the Peierls barrier value from the Bordoni peak measurements [4], the microscopic meachanisms of this peak are not known in detail.In the next chapter, the behaviour of anelastic materials will be introduced in order to understand the internal friction measurements, then in chapter 3, the effects of the lattice periodicity on dislocations will be presented. Undestanding this will be important to introduce the concept of the Peierls barrier which generates the anelastic effects due to dislocations. Then in chapter 4 we finally introduce the phenomenology of the Bordoni peak. The final chapter corresponds to the actual work done in this thesis, where molecular dynamics simulations were done in copper to find the Bordoni peak in order to shed light on the microscopic causes of this effect.

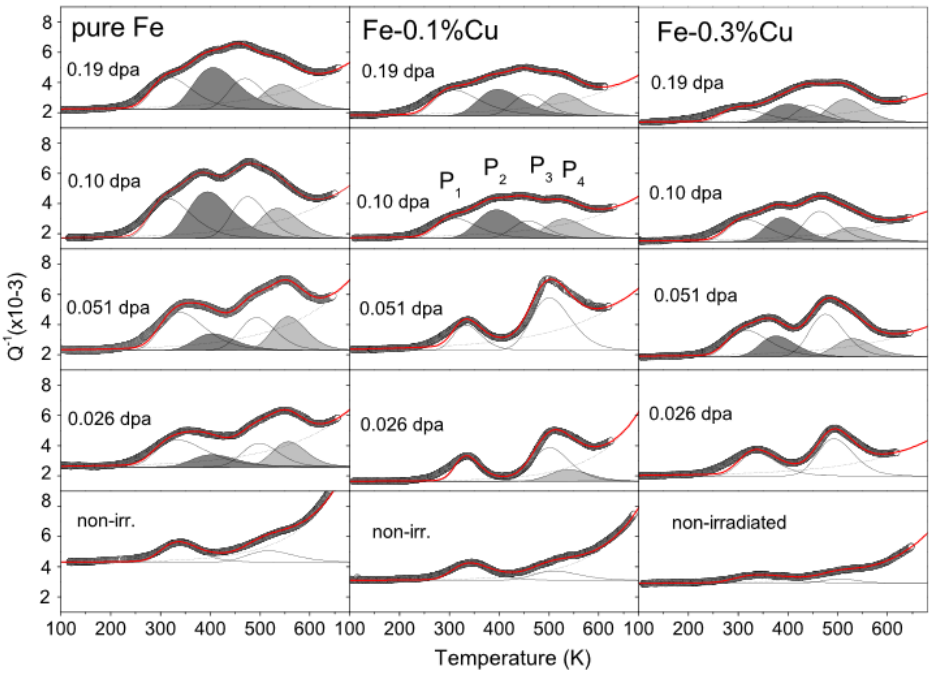

Figure 1.3: Measure of internal friction vs temperature of Cu and Fe alloy in different concentrations and different neutron radiation levels. From this measurements it is possible to deduce mechanical properties of materials such as the presence of defects in the crystal structure. Image taken from [5].

Chapter 2

Elasticity and anelasticity in solids

In this chapter we will make a small revision of the elastic regime in solids to then introduce the anelastic regime and how it deviates from ideal elasticity which will be relevant to this work. This chapter follows closely reference [4]. This introduction is done with the objective of presenting the dissipation of energy in anelastic solids, which are relevant to understand for the molecular dynamics simulations done in this thesis

2.1 Ideal Elasticity

In an elastic solid it is known that Hooke's law is verified between the stress σ and the strain ε:

$$\sigma = M\varepsilon \tag{2.1}$$

$$\varepsilon = J\sigma \tag{2.2}$$

The constant M is called the elastic modulus, for arbitrary stresses and strains both variables are expressed as tensors of rank 2 where the components of these two tensors are related by lineal equations. For the purpose of introducing anelasticity we will just consider equation as a simple linear relation rather than tensors. This implies that we are considering pure shear stresses, uniaxial deformations o hydrostatic deformation.

There are three main assumptions in equations (2.1) and (2.2):

1. There is a unique equilibrium relation between stress and strain.
2. The equilibrium response is achieved instantaneously. When a sound wave is present, the response can be considered instantaneous in an infinitesimally small region.
3. The response is linear.

	Unique equilibrium relation	Instantaneous response	Lineal
Ideal elasticity	Yes	Yes	Yes
Non lineal elasticity	Yes	Yes	No
Instantaneous plasticity	No	Yes	No
Anelasticity	Yes	No	Yes
Viscoelasticity	No	No	Yes

Table 2.1: Summary of the classification of the different elastic regimes in solids. Unique equilibrium relation means that there is a unique equilibrium relation between stress and strain. Instantaneous response means that the equilibrium relation between stress and strain is achieved instantaneously. Lineal means that there is a lineal relation between stress and strain.

2.2 Anelasticity

If we relax any of the three conditions mentioned in the previous section, we will obtain different regimes whose characteristics are summarized in table 2.1. From the table we can see that anelasticity is defined by relaxing the condition of instantaneous response. In the next section we will see that when a strain or a stress is applied, anelastic relaxation can appear. This relaxation when it is present, is due to other internal variables in the sample, coupled to the strain and stress of the material. A simple system where this kind of relaxation occurs is in a spring with a complex spring constant k, another analogous system is a dielectric subject to an alternating external electric field. In this last example the permittivity will be a complex number and the response of it will lag behind the forcing of the oscillatory electrical field.

2.2.1 Anelastic relaxation

Anelastic relaxation can be illustrated through a simple example. Suppose at time $t = 0$ a constant stress σ_0 is applied to a solid and is kept constant from then on:

$$\sigma = \begin{cases} \sigma_0 & \text{if } t \geq 0 \\ 0 & \text{if } t < 0 \end{cases} \tag{2.3}$$

If subsequently, the strain is measured in the sample, then the strain response will be a function of time $\varepsilon(t)$. From linearity we know that $\varepsilon(t)/\sigma_0$ is independent of σ_0, so we can define a response function

$$J(t) = \varepsilon(t)/\sigma_0$$

Note that for the elastic case $J(t)$ becomes the constant J defined in equation 2.2. The initial value $J(0) = J_U$ is called the unrelaxed compliance and it corresponds to the instantaneous part of the response. We also define the relaxed compliance $J(\infty) = J_R$ and the relaxation of the compliance as their difference $\delta J = J_R - J_U$.

We compare qualitatively the behaviour of ideal elasticity, anelasticity and viscoelasticity

under the applied stress as defined above, in figure 2.1 (taken from [4]). From the figure we can also see what happens when the constant stress is removed. Anelasticity is characterized by an instantaneous response related to the elastic properties of the material and an anelastic relaxation response related to anelasticity. In the case of viscoelasticity it is seen that there is no a unique equilibrium relation. This can be noted in the so called creep which is the tendency to deform permanently under the influence of stress, this effect can be seen in figure 2.1.

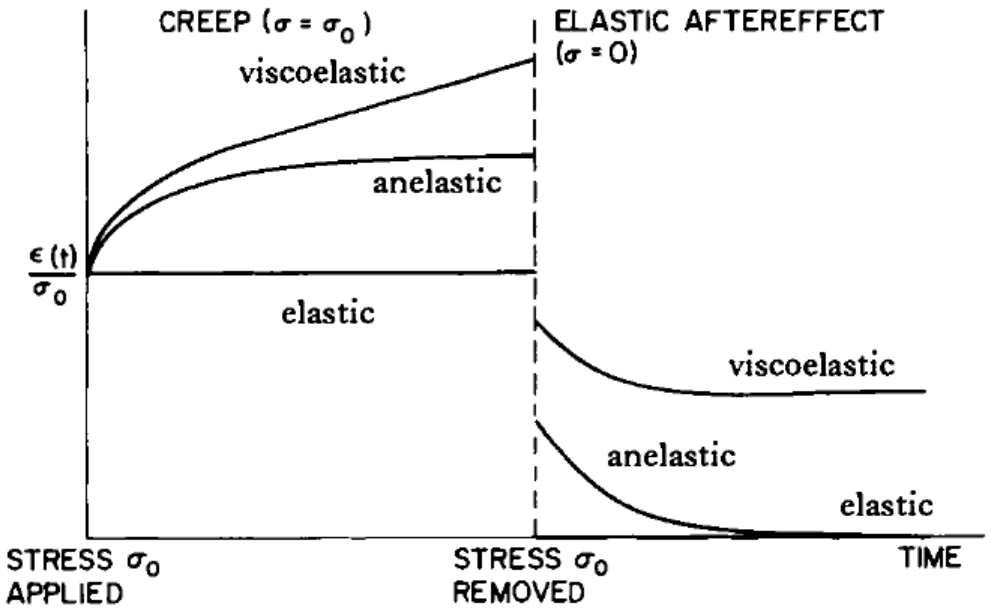

Figure 2.1: Qualitative response of the strain when a constant stress is applied to a solid, in the cases of elastic, anelastic and viscoelastic solids. Notice that anelastic solids have an elastic instantaneous response and also a retarded response. This behaviour is further explained in the text. (Figure modified from [4]).

2.2.2 Anelastic dynamic response

Suppose now that instead of applying a constant stress, an stress oscillatory in time with angular frequency ω is imposed on the anelastic sample. We can describe the stress as

$$\sigma(t) = \sigma_0 \mathrm{e}^{\mathrm{i}\omega t} \tag{2.4}$$

where σ_0 is the stress amplitude and ω the angular frequency. The condition of linearity implies that the strain response is periodic with the same frequency but with a phase difference

$$\varepsilon(t) = \varepsilon_0 \mathrm{e}^{\mathrm{i}(\omega t - \phi)} \tag{2.5}$$

where ε_0 is the strain amplitude and ϕ is the phase by which the strain lags behind the stress. In general they are both functions of ω. Note that linearity also implies that ε_0/σ_0 is independent of σ_0.

Next we define a function called the complex compliance,

$$J = \varepsilon/\sigma = \mid J \mid (\omega)\mathrm{e}^{-\mathrm{i}\phi(\omega)},$$

where $\mid J \mid = \varepsilon_0/\sigma_0$. From the two response functions just defined, J and ϕ, we can define two other functions. To this end we write equation (2.5) in an alternative form

$$\varepsilon = (\varepsilon_1 - \mathrm{i}\varepsilon_2)\mathrm{e}^{\mathrm{i}\omega t}$$

where ε_1 is the strain amplitude of the in-phase with stress component and ε_2 is the 90° out of phase amplitude. Dividing by σ we obtain

$$J(\omega) = J_1(\omega) - \mathrm{i}J_2(\omega)$$

where $J_1 = \varepsilon_1/\sigma$ y $J_2 = \varepsilon_2/\sigma$. J_1 is then the real part of J and J_2 is the imaginary part. Note that

$$\mid J \mid = J_1^2 + J_2^2$$

$$\tan\phi = J_2/J_1.$$

J_1 is called the storage compliance and J_2 the loss compliance. To understand the origin of this name we calculate the energy dissipated in a full cycle per unit volume. Since σ and ε are out of phase there will be a hysteresis loop in the stress-strain plot, its surface is interpreted as the energy lost in a cycle, and it's given by

$$\Delta W = \oint \sigma \mathrm{d}\varepsilon = \pi J_2 \sigma_0^2$$

where the integral is performed over one period. This shows that J_2 is proportional to the energy lost in one cycle. In an analogous way we can calculate the maximum stored energy W per unit volume, integrating over one quarter of a period:

$$W = \int_{\omega t=0}^{\pi/2} \sigma \mathrm{d}\varepsilon = \frac{1}{2} J_1 \sigma_0^2$$

If we calculate the ratio of both quantities defined above we obtain

$$\frac{\Delta W}{W} = 2\pi J_2/J_1 = 2\pi \tan\phi \tag{2.6}$$

The ratio of the dissipated energy in one cycle and the maximum energy stored is called the fractional energy loss per cycle due to the anelastic behaviour. From this ratio we define the internal friction Q^{-1}

$$Q^{-1} = \frac{\Delta W}{2\pi W} = \tan\phi \tag{2.7}$$

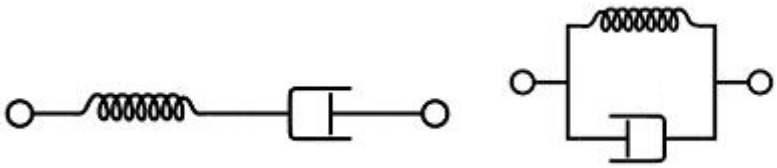

(a) Maxwell Model (b) Voigt Model

Figure 2.2: An schematic figure of Maxwell and Voigt model

2.2.3 Mechanical models of anelasticity

In this section a simple mechanical model capable of demonstrating anelastic behaviour will be shown and in this way a simple relation between stress and strain in the anelastic regime will be found.

From the assumption of linearity and time dependence (non instantaneous) the most general relation between stress and strain is

$$a_0\sigma + a_1\dot{\sigma} + a_2\ddot{\sigma} + ... = b_0\varepsilon + b_1\dot{\varepsilon} + b_2\ddot{\varepsilon} + ... \tag{2.8}$$

In order to describe anelasticity we first review some simple mechanical models. If all the coefficients except a_0 and b_0 are zero we recover Hooke's law. Another mechanical model that can be described is the dashpot with a viscous response, whose equation is $\sigma = \nu\dot{\varepsilon}$ (all coefficients are 0 except $a_0$and b_1). We can also form mechanical models by combining the ideal spring and the dashpot. To do this, notice that when combining in series two elements the stresses σ_1 and σ_2 are equal while the strains ε_1 and ε_2 are additive.

$$\varepsilon = \varepsilon_1 + \varepsilon_2$$

$$\sigma = \sigma_1 = \sigma_2$$

Whereas for combinations in parallel we have

$$\varepsilon = \varepsilon_1 = \varepsilon_2$$

$$\sigma = \sigma_1 + \sigma_2$$

One known model is the Voigt model which is composed of a spring and a dashpot in parallel, another one is called the Maxwell model, composed of an spring and a dashpot in series, see figure 2.2. If a stress σ_0 is applied at $t = 0$, the dashpot won't yield instantaneously but it will start to flow after some time. At $t = \infty$ the stress will become entirely sustained by the spring. When the stress applied is taken away the dashpot will begin creeping back to its position because of the force generated by the extended spring. Figure 2.3 represents the situation.

The equation of the situation presented above is obtained considering that $\varepsilon_1 = J\sigma_1$ for the spring and $\varepsilon_2 = J\sigma_2/\tau$ for the dashpot. Following the rules of elements in parallel we get the equation

$$J\sigma = \varepsilon + \tau\dot{\varepsilon}$$

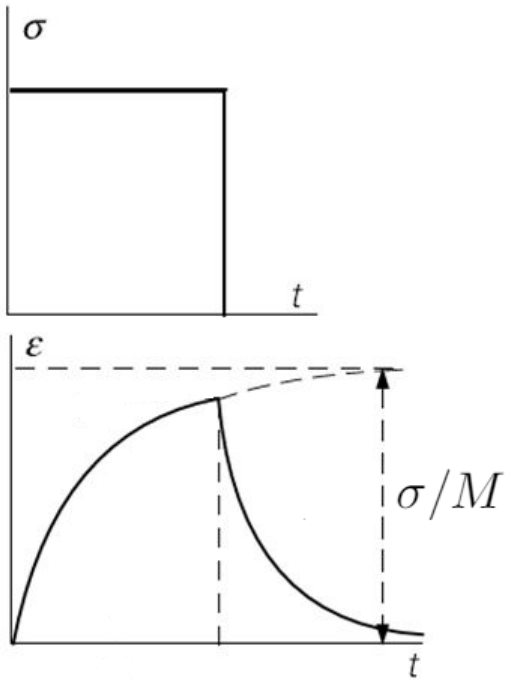

Figure 2.3: Qualitative behaviour of the strain response in the Voigt model for a constant applied stress during a finite time interval. When the applied stress is taken away the dashpot will begin creeping back to its position because of the force generated by the extended spring. When the stress is turned off there is a relaxation time needed to get back to equilibrium.

This equation is equivalent to equation (2.8) with a_0, b_0 and b_1 different from 0. Solving this equation we get the behaviour shown in the figure 2.3.

From the analysis of the Voigt model we see that we can explain the relaxation which is characteristic in anelasticity, but notice that in figure 2.1 there is an elastic component in the response, we still need to explain the elastic part of the response. To add the elasticity we can just add in series a spring to the Voigt model. In this way we obtain a behaviour similar to the anelastic case in figure 2.1. The mechanical model is shown in figure 2.4

Since the system of figure 2.4 has the characteristics of an anelastic material, the solution will be relevant to this work. Using the notation in the figure and considering $\varepsilon_a = J_U\sigma_a$, $\varepsilon_b = \delta J\sigma_b$ and $\dot{\varepsilon_c} = \delta J\sigma_c/\tau_\sigma$ we can obtain the stress-strain relation:

$$J_R\sigma + \tau_\sigma J_U\dot{\sigma} = \varepsilon + \tau_\sigma\dot{\varepsilon} \tag{2.9}$$

where $J_U + \delta J = J_R$. Now we consider an oscillatory stress on the model $\sigma = \sigma_0 e^{i\omega t}$ and a strain response as in the anelastic case $\varepsilon = (\varepsilon_1 - i\varepsilon_2)e^{i\omega t}$. Substituting the strain and stress in equation 2.9 we arrive to the equations

$$J_R = J_1 + \omega\tau_\sigma J_2$$

$$\omega\tau_\sigma J_U = \omega\tau_\sigma J_1 - J_2$$

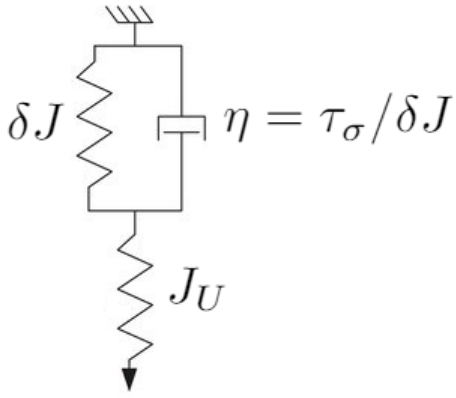

Figure 2.4: Mechanical model of the Voigt model. The model consists of a spring and a dashpot in parallel and one spring in series with the first two. J_U, δJ and η are defined in the text.

and solving for J_1 and J_2 we obtain

$$J_1(\omega) = J_U + \frac{\delta J}{(1+\omega^2\tau_\sigma^2)}, \tag{2.10}$$

$$J_2(\omega) = \delta J \frac{\omega\tau_\sigma}{(1+\omega^2\tau_\sigma^2)}. \tag{2.11}$$

A plot of equations (2.10) and (2.11) is shown in figures 2.5 and 2.6. When $\omega\tau_\sigma = 1$ there is

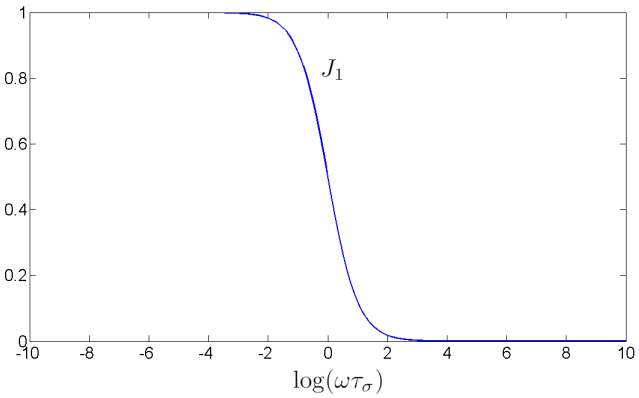

Figure 2.5: Function J_1 with $J_U = 0$ and $\delta J = 1$ from equation 2.10.

a peak in the J_2 function. This means, according to equation (2.6) that there is a maximum in the dissipated energy when the system is forced at the frequency $\omega = 1/\tau_\sigma$, this will be relevant in chapter 4. This last remark is evident if we notice that the internal friction can be written as

$$\tan\phi = \frac{J_2}{J_1} = \delta J \frac{\omega\tau_\sigma}{J_R + J_U\omega^2\tau_\sigma^2}. \tag{2.12}$$

The expression for the internal friction has the same dependence on ω and τ_σ as J_2.

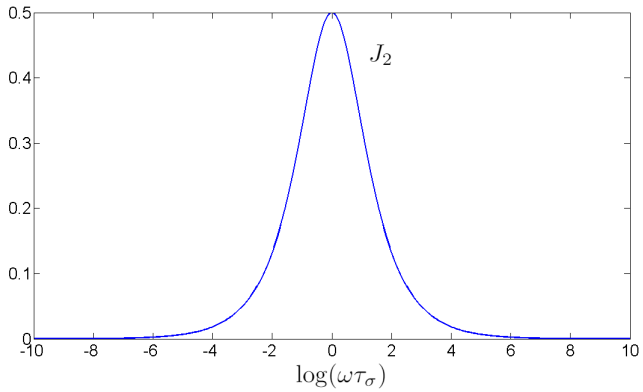

Figure 2.6: Function J_2 with $J_U = 0$ and $\delta J = 1$ from equation 2.11. Notice that the maximum occurs when $\omega = \tau_\sigma^{-1}$.

2.2.4 Origin of anelastic behaviour

In the last subsections time dependent behaviour has been included in Hooke's law in order to understand anelastic response, but the origin of this behaviour in solids has not been mentioned yet. In this subsection the origin of such behaviour will be studied.

The reason for the delay between stress and strain can be understood as the coupling of an internal variable to the stress and strain in the sample. An example of an internal variable can be the displacements of dislocations, this will be seen in detail in section 4.

In general, let us suppose there is a single variable ξ, the internal variable, coupled to the stress σ and strain ε according to equation

$$\varepsilon(\sigma, \xi) = J_U\sigma + \chi\xi \tag{2.13}$$

where χ is a coupling between ξ and ε. In this way the total strain is expressed as the sum of two terms, the first one is the known Hookes law, and the second is defined as the anelastic strain $\varepsilon_{ane} = \chi\xi$. Now the state of the system will be described by ε, σ and ξ. Equation (2.13) assumes that the relation between this variables is linear. A second assumption is that there is an equilibrium value of ξ for each σ which we will call $\bar{\xi}$, and they are also linearly related.

$$\bar{\xi} = \mu\sigma. \tag{2.14}$$

In general μ depends on the temperature. The final assumption is that ξ approaches its equilibrium value over a period of time, in the case of dislocations mentioned above this delay may be caused by their interaction with impurities in the crystal or the roughness of the potential the dislocation is subject to.

Only a first order approximation is needed to see the effects of the new internal variable on the anelastic response: A first order equation for $\frac{\mathrm{d}\xi}{\mathrm{d}t}$ is

$$\frac{\mathrm{d}\xi}{\mathrm{d}t} = -\frac{1}{\tau}(\xi - \bar{\xi}). \tag{2.15}$$

where τ is the coefficient of the first order approximation, which has units of time. If this equation is solved for ξ then τ will represent a relaxation time. Substituting equation (2.14) in (2.13) and comparing with the equation 2.9 we obtain

$$\delta J = \bar{\varepsilon}_{ane}/\sigma = \chi\bar{\xi}/\sigma = \chi\mu$$

Thus we connect the mechanical models with parameters related to the internal variable. For more conections with the mechanical model and equation (2.9) see [4].

2.2.5 Properties of the anelastic solid as function of temperature

In the previous subsection properties such as J_1 and J_2 were plotted against $\log \omega\tau$. Properties like these or like $\tan\phi$ take particular forms when plotted this way. In experiments where the sample is subject to oscillatory stress or strain, for example sound waves, the frequency ω is a parameter that is varied while the relaxation time τ is constant. The problem is that the peaks obtained imply that the frequency needs to vary over two decades. In torsio pendulum experiments varying the frequency is impractical [4], so another alternative must be sought if these peaks want to be studied.

Another option is naturally to vary τ while keeping ω constant. This method is the one usually used and it will be discussed in this subsection.

In most of the cases the relaxation rate τ^{-1} has an Arrhenius type dependence on the temperature, that is to say

$$\tau^{-1} = \nu_0 \mathrm{e}^{-\frac{A}{kT}} \tag{2.16}$$

where T is the absolute temperature, ν_0 is a frequency factor, A is an activation energy and k is Boltzmann's constant. This equation for τ^{-1} is valid when the relaxation process involves the movement over an energy barrier. Alternatively, 2.16 can be written as

$$\tau = \tau_0 \mathrm{e}^{\frac{A}{kT}}, \tag{2.17}$$

with $\tau_0 = \nu_0^{-1}$. From the last relation we see that τ may be changed in a wide range by varying T because of the exponential relation. Therefore by substituting equation (2.17) in the equations (2.10) and (2.11) it is possible to obtain the dependence of the variables in an anelastic solid with temperature. From 2.17 we see also that

$$\ln \omega\tau = \ln \omega\tau_0 + \frac{A}{kT}$$

and there is a linear relation between $\ln \omega\tau$ and the inverse of the temperature. This implies that a graph that dependends on $\frac{A}{kT}$ has the same form as one that depends on $\ln \omega\tau$, but with a shift in the horizontal axis. In many experiments of internal friction the graphs are expressed in terms of $1/T$ for this reason.

Chapter 3

Influence of lattice periodicity on dislocations

In this chapter the effects of the discreetness of the lattice on the dislocation will be shown. This, with the objective of introducing the Peierls barrier which has been the source of many discussions because of the discrepancies of its measurement in experiments, this discrepancy will be commented in the next chapter.

Dislocations are line defects in periodic crystals. In continuous mechanics, dislocations are typically described as lines in a homogeneous solid [7]. This is of course a macroscopic scale description. In real crystals however, we have lattice periodicity which affects the behaviour of these defects. For instance in the Frenkel treatment of the shear strength of a perfect crystal a periodic potential energy of displacement is considered (see chapter 1 of [2]). We can expect then that a similar periodic potential will affect the movement of dislocations.

A simple model, initially applied to the movement of dislocations in periodic potentials, is the Frenkel-Korontova model (see chapter 8 of [2]) which consists of a one dimensional array of masses connected by springs lying on a periodic potential. Subsequent developments of this phenomenological model allowed qualitative descriptions of the slip process in dislocations.

A more realistic solution was first made by Peierls [8] and later refined by Nabarro [9]. Their model is useful for the calculation of the dislocation width and for estimating the core energy of a dislocation. It is also used to calculate the lattice displacement potential that resists dislocation motion and the associated stress as will be explained later, although there are still problems to connect this predictions with experiments. In the next subsection we present the model known as Peierls-Nabarro dislocation model.

3.1 Peierls-Nabarro dislocation model

In continuous mechanics dislocations are considered as strings embedded in an elastic medium. It is possible to calculate the stress field generated by edge or screw dislocations in the con-

tinous approximation [2], [10]. In the case of the edge dislocation we have for example the shear stress field, with the dislocation line pointing in the z direction:

$$\sigma_{xy}(x,y) = \frac{\mu b}{2\pi(1-\nu)} \frac{x(x^2-y^2)}{(x^2+y^2)^2}.$$

where ν is Poisson's ratio, μ is the shear modulus and b is the Burgers vector. Notice that at the origin $x, y = 0$ the stress field has an artificial divergence. This is due to the continuous approximation that doesn't take into account the discrete nature of the crystal lattice. In the following subsection the stress and displacements generated at the core of the dislocation will be obtained, and afterwards the potential "seen" by the dislocation will be calculated from this model to define the Peierls stress, a quantity related to the mechanical properties of materials.

3.1.1 Stress and displacement in the core

We will present this model in a simple cubic lattice of lattice constant b as was originally done by Peierls and Nabarro. Consider first two simple cubic half-infinite lattices, with their cubic axes parallel, separated by a distance d as shown in figure 3.1.

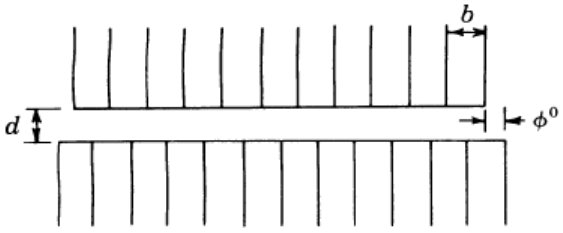

Figure 3.1: Schematic illustration of two semi-infinite simple cubic crystals with a displacement of $b/2$. The vertical lines represent columns of atoms. The disregistry in this case is $b/2$ where b is the Burgers vector. This is because the difference in distance between one row in the upper plane and the lower one is $b/2$. This disregistry defines a dislocation (Figure taken from [2]).

We can define the disregistry ϕ_x^0 of the upper lattice with respect to the bottom one as

$$\phi_x^0 = \begin{cases} b/2 & \text{if } x \geq 0 \\ -b/2 & \text{if } x < 0 \end{cases} \tag{3.1}$$

where b is the Burgers vector and the line of the edge dislocation points inside the page (see figure 3.2). If the upper and lower part of the crystal are joined, we obtain figure 3.2. An edge dislocation will form in the crystal. In this second case the disregistry will be

$$\phi_x^0 = \begin{cases} 2u_x(x) + b/2 & \text{if } x \geq 0 \\ 2u_x(x) - b/2 & \text{if } x < 0 \end{cases} \tag{3.2}$$

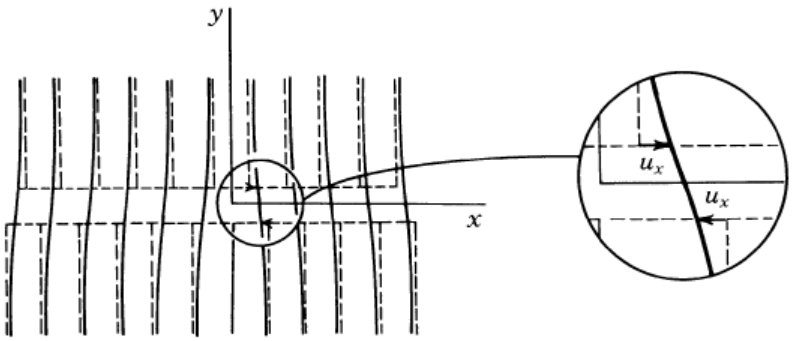

Figure 3.2: Cubic crystal with a disregistry of $b/2$. In the origin there is a dislocation due to the displaced atoms. The continous lines represent the rows of atoms, notice that when the upper and lower plane come together there is a strain on the atoms near the dislocation (Figure taken from [2])

The atoms in the upper crystal are subject to two forces [9]: first due to the interaction with the atoms in the same upper crystal, and a second force due to the interaction with atoms in the bottom crystal. The first force tends to spread the compression dut to the strains caused by the disregistry and the second force tends to bring the atoms in the upper part in alignment with the lower atoms. If we define a dislocation width in this sample (it will be defined quantitatively later), the first force will tend to increase the width and the second will shorten it. The competition between both forces will create a characteristic size of the dislocation width [10].

We assume here that the dislocation size is large compared to the interatomic distance, the vertical and horizontal displacements vary slowly from atom to atom. From this assumption Peierls and Nabarro treat both half crystals as isotropic elastic media.

These forces associated to the distorted bonds imply a local stress in the plane $y = 0$. If we assume that horizontal forces are only due to difference in displacements in the x axis and consider the periodic nature of the crystal, then the stress generated by these forces can be expressed as

$$\begin{aligned} \sigma_{xy}(x,0) &= K \sin(\frac{2\pi\phi_x}{b}) \\ &= -K \sin(\frac{4\pi u_x}{b}) \end{aligned} \tag{3.3}$$

The second equality is obtained by substitution with the definition of ϕ_x. The constant K is obtained by imposing that Hooke's law is verified by the stress.

$$\begin{aligned} \sigma_{xy}(x,0) &= 2\mu\varepsilon_{xy} \\ &= \frac{\mu\phi_x}{a} \end{aligned} \tag{3.4}$$

where a is the interatomic distance. Using equations (3.3) and (3.4) we obtain

$$\sigma_{xy}(x,0) = -\frac{\mu b}{2\pi a} \sin(\frac{4\pi u_x}{b}) \tag{3.5}$$

Now we wish to calculate the energy related to the presence of the dislocation. As was mentioned in section 3.1 we want to obtain the energy that the dislocation is subject to, for this we compute the energy related to the presence of the dislocation so, thus, the stress and displacements generated by the dislocations must be calculated. We have obtained the stress, we still need to calculare the deformation u_x. Following Eshelby [11], the dislocation defined with a Burgers vector b is described as a continuous distribution of infinitesimal Burgers vectors that lie in the x axis line. This fact will be used in the following calculations.

It is known that dislocations are related to displacements in the crystals through [7]

$$\begin{aligned} \oint \mathrm{d}u_{\mathrm{i}} &= \oint \frac{\partial u_{\mathrm{i}}}{\partial x_k} \mathrm{d}x_k \\ &= -b_{\mathrm{i}} \end{aligned} \tag{3.6}$$

In fact this equation is used to define the Burgers vector of a dislocation. When a dislocation is circled around, the displacement from the initial point to the finishing point of the circuit is defined as the Burgers vector. The displacement generated by the infinitesimal Burgers vectors is identified as $b'(x') = -2\frac{\mathrm{d}u_x}{\mathrm{d}x}\mathrm{d}x'$[11] and since we know that the Burgers vector of the dislocation is b then we impose

$$\begin{aligned} b &= \int_{-\infty}^{\infty} b'(x')\mathrm{d}x' \\ &= -2\int_{-\infty}^{\infty} (\frac{\mathrm{d}u_x}{\mathrm{d}x})_{x=x'}\mathrm{d}x' \end{aligned} \tag{3.7}$$

where b' is the infinitesimal vector Burgers distribution. Since the shear stress field generated by a dislocation is [2]

$$\sigma_{x,y}(x,y) = \frac{\mu b}{2\pi(1-\nu)} \frac{x(x^2-y^2)}{(x^2+y^2)^2}$$

where ν is Poisson's ratio, we can derive a similar result for the infinitesimal dislocation distribution

$$\begin{aligned} \sigma_{xy}(x,0) &= -\frac{\mu}{2\pi(1-\nu)} \int_{-\infty}^{\infty} \frac{b'\mathrm{d}x'}{x-x'} \\ &= \frac{\mu}{\pi(1-\nu)} \int_{-\infty}^{\infty} \frac{(\mathrm{d}u_x/\mathrm{d}x)_{x=x'}\mathrm{d}x'}{x-x'} \end{aligned} \tag{3.8}$$

Notice that the stress in equation 3.5 is the stress due to the deformation of the bonds and stress in equation 3.8 is due to the stress field generated by the edge dislocation in the crystal. In equilibrium, both stresses should be equal and in opposite directions. Thus, equating both we have

$$\frac{\mu}{\pi(1-\nu)} \int_{-\infty}^{\infty} \frac{(\mathrm{d}u_x/\mathrm{d}x)_{x=x'}\mathrm{d}x'}{x-x'} = \frac{\mu b}{2\pi a} \sin(\frac{4\pi u_x}{b}) \tag{3.9}$$

This equation can be solved for u_x ([11], [12]), the solution is

$$u_x = -\frac{b}{2\pi} \tan^{-1} \frac{x}{\xi} \tag{3.10}$$

where $\xi = \frac{a}{2(1-\nu)}$ (recall the d is the interatomic distance). The width of the dislocation is defined as 2ξ. The function obtained can be seen in figure 3.3 Substituting equation (3.10)

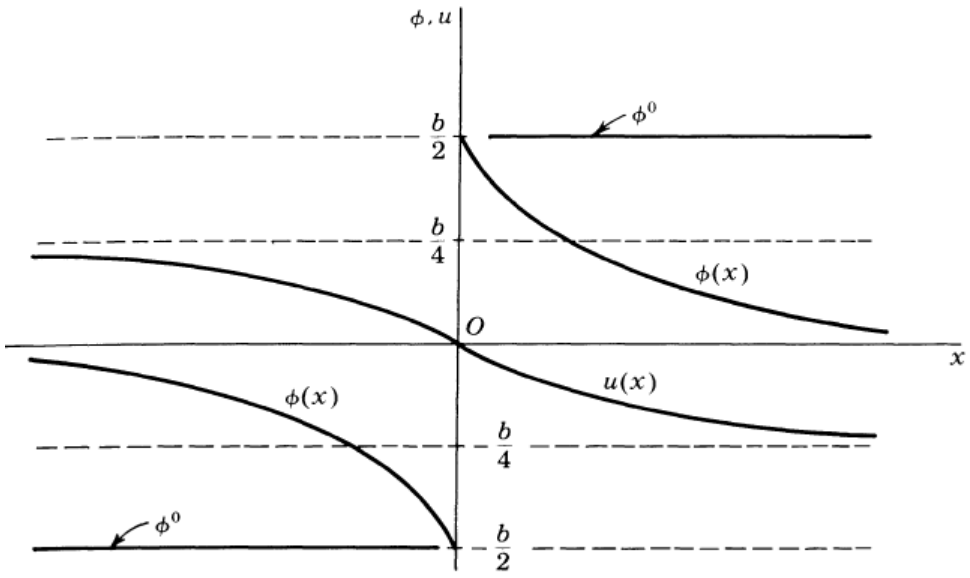

Figure 3.3: Schematic plot of displacement function u and diresgistry ϕ. Notice that from the behaviour of this functions it is possible to define a width for the dislocation since there is a characteristic length in the function u (Figure taken from [2]).

in equation (3.8) we obtain the result

$$\sigma_{xy}(x,0) = -\frac{\mu b}{2\pi a}\frac{x}{x^2+\xi^2} \tag{3.11}$$

If we had not considered the core effects of the lattice periodicity, the obtained stress would have diverged in the origin, but with Peierls and Nabarro calculation it is possible to estimate the value of the stress in the core. The stresses obtained though are large and it is questionable whether Hooke's law applies.

3.1.2 Elastic energy in Peierls Nabarro model

Now that the stress and displacements in the core of the dislocation have been obtained, it is possible to calculate the effective potential that the dislocation is subject to. To do this the elastic energy stored because of the dislocation will be obtained.

Two energies, associated with the dislocation can be defined. One is related to the stress field generated by the dislocation and stored in both half crystals (the energy related to the dislocation treated as a line), and another one related to the distorted bonds in the $y = 0$ half-plane (the energy related to the core of the dislocation). The latter usually called the misfit energy. Since the Peierls Nabarro model treats the displacements as continuous, this division is artificial but consistent with the calculations of the last subsection.

The elastic strain energy in both half crystals is equal to the work done by the stress to generate the displacements u_x. In an element of area (δx) times (unit length in z direction)

the work is

$$\delta W = \int_0^{u_x} \sigma_{xy}(x,y)\,\delta x\,\mathrm{d}u = \sigma_{xy}(x,0)\,\delta x\,u_x.$$

Substituting u_x and σ_{xy} by equations (3.10) and (3.11) and integrating from $x=-r$ to $x=r$ we have

$$W = \int_{-r}^{r} \sigma_{xy}u_x = \frac{\mu b^2}{4\pi^2(1-\nu)}\int_{-r}^{r}\frac{x\tan^{-1}(\frac{x}{\xi})}{x^2+\xi^2}\mathrm{d}x = [\frac{1}{2}\ln(1+z^2)\tan^{-1}z]_{-r/\xi}^{r/\xi} - \frac{1}{2}\int_{-r/\xi}^{r/\xi}\frac{\ln(1+z^2)\mathrm{d}z}{1+z^2}$$

where the last equality is obtained with the change of variable $z=x/\xi$ and integration by parts. In the limit $r >> \xi$ the first term reduces to $\pi\ln(r/\xi)$ and the second term can be evaluated by complex integration obtaining $-\pi\ln 2$. Thus,

$$W = \frac{\mu b^2}{4\pi(1-\nu)}\ln(r/2\xi). \tag{3.12}$$

Now the misfit energy is calculated. The shear strain on the slip surface $y=0$ is

$$\varepsilon_{xy}(x,0) = -\frac{\phi_x}{2a} = -\frac{2u_x+(b/2)}{2a}.$$

The strain energy is calculated considering $\sigma_{xy}\mathrm{d}\varepsilon_{xy} + \sigma_{xy}\mathrm{d}\varepsilon_{yx} = 2\sigma\mathrm{d}\varepsilon_{xy}$. In an element of height a, width δx and unit length depth, the energy is

$$\delta W = -2\int a\,\delta x\,\sigma_{xy}\,\mathrm{d}\varepsilon_{xy} = 2\int_{b/4}^{u_x}\delta x\,\sigma_{xy}\mathrm{d}u_x.$$

The negative sign in the second equality is due to the sign of the stress to generate such strain. The stress in the last equation is in fact the stress defined in equation (3.3). Remember that this stress is the one generated by the distorted angles, so this explains the negative sign. The integration starts from $b/4$ because this is the disregistry in the $y=0$ plane when there are no forces on the half planes. Substituting the definition of σ_{xy} from equation 3.5 in the last equation we obtain

$$\begin{aligned}\delta W &= -\frac{\mu b\delta x}{\pi a}\int_{b/4}^{u_x}\sin\frac{4\pi u_x}{b}\mathrm{d}u_x \\ &= \frac{\mu b^2\delta x}{4\pi^2 a}(1+\cos\frac{4\pi u_x}{b})\end{aligned} \tag{3.13}$$

and the total misfit energy is

$$W_m = \frac{\mu b^2}{4\pi^2 a}\int_{-\infty}^{\infty}(1+\cos\frac{4\pi u_x}{b})\mathrm{d}x = \frac{\mu b^2}{4\pi(1-\nu)}. \tag{3.14}$$

Notice that until now the calculation of the energy has been done using only continuous mechanics. In particular it is obtained that the misfit energy is a constant in the slip plane of the dislocation. If we were to consider the lattice periodicity, then the expected result would be an oscillating energy on which the dislocation would glide. The reason for this discrepancy between the constant energy result and the expected oscillatory result is due to the smearing out of the discrete atoms in the lattice.

Instead of the misfit energy calculation above, a sum will be made of the misfit energy per row of atoms on one side of the crystal, this sum will be over all rows on both surfaces. In this way we are taking into account the discrete nature of the lattice. Consider the misfit energy calculated in (3.13), this energy divided by 2 is the misfit energy per row in one half of the crystal and $\delta x = b$ because of the discrete lattice

$$\begin{aligned} W(x) &= \frac{\mu b^3}{8\pi^2 a}(1 + \cos\frac{4\pi u_x}{b}) \\ &= \frac{\mu b^3}{4\pi^2 a}\frac{\xi^2}{\xi^2 + x^2}. \end{aligned} \tag{3.15}$$

In the last equality the trigonometric identity $\cos(2\theta) = \frac{1-\tan^2\theta}{1+\tan^2\theta}$ and result (3.10) were used. If we calculate the total energy, integrating over all the real line, we obtain:

$$W = \frac{\mu b^3}{4\pi^2 a}\pi\xi$$

This result implies that if we consider the atoms of the crystal as a continuous distribution, then the energy related to the position of the dislocation smears out since the result is just a constant. If instead in equation (3.15) the variable x is a discrete variable which designates the position of the rows in the surface between the half crystals, that is to say, $x = \frac{b}{2}n$ with n an integer. Notice that the bottom half crystal rows correspond to n even and the top half crystal rows corresponds to n odd. Then we have

$$W = \frac{\mu b^3}{4\pi^2 a}\sum_{n=\infty}^{\infty}\frac{\xi^2}{\xi^2 + (\frac{b}{2}n)^2}.$$

When the dislocation is translated a distance $b\alpha$, where α is an arbitrary real number, every row gets translated by the same distance. So, if we consider the translation of the dislocation by $b\alpha$ the energy is

$$W = \frac{\mu b^3 \xi^2}{\pi^2 a b^2}\sum_{n=\infty}^{\infty}\frac{1}{(2\xi^2/b)^2 + (2\alpha + n)^2}.$$

It can be shown that this sum is finite and that the result is [13]

$$W(\alpha) = \frac{\mu b^2}{4\pi(1-\nu)} + \frac{\mu b^2}{2\pi(1-\nu)}\exp(-\frac{4\pi\xi}{b})\cos(4\pi\alpha) = \frac{\mu b^2}{4\pi(1-\nu)} + \frac{W_p}{2}\cos(4\pi\alpha). \tag{3.16}$$

W_p is called the Peierls energy. Notice that as α changes (the dislocations translates) the energy oscillates as expected. This can be interpreted as an energy potential on which the dislocation moves, thus it is possible to calculate the stress to surmount the energy barrier into the next minimum with

$$\tau_p = \frac{1}{b^2}(\frac{\partial W}{\partial \alpha})_{max} = \frac{2\pi W_p}{b^2} = \frac{2\mu}{1-\nu}\exp(-\frac{4\pi\xi}{b}) \tag{3.17}$$

This quantity is called the Peierls stress. The first equality is obtained by considering the work needed to get to the maximum of the barrier. Eventhough the Peierls model fails to predict quantitavely the Peierls stress (see references mentioned in section 4). The qualitative features of the model are correct. Notice that wider and more planar core structure of the dislocation implies lower Peierls stress. Peierls energy can be very anisotropic in a crystal, dislocations will tend to align along the most closely-packed directions [14], for which τ_p is maximum. For instance this direction in the FCC crystal is the $\langle 111\rangle$ direction.

3.1.3 Criticism to Peierls Nabarro Model

The first thing to be noted is that the model only considers planar cores in simple cubic lattices, there are cases when non collinear dissociation can exist. This can happen for example in FCC crystals with partial dislocations, where the Burgers vector of the Shockley partials is non collinear with the $\langle 111 \rangle$ direction. Other assumptions that are criticized are the use of continuous mechanics considering the presence of the discrete lattice and that the model only applies at 0 K .

There have been subsequent modifications to this model, for example phenomenological force laws have been included to approximate the lattice nature of the crystal [2]. The role of temperature has been considered in other models (see page 238 of [2]).

Chapter 4

The Bordoni peak

In this chapter the phenomenology of the Bordoni Peak is presented. The theory about the production of this peak is also presented and finally comments will be made on the discrepancy of the Peierls barrier in different experiments.

A dislocation always produces a strain field inside a crystal and when a stress is applied in the crystal the dislocation is displaced, in this way the dislocation displacement is coupled to the strain and the stress in the sample. It is because of this coupling that dislocation displacement can be considered an internal variable in the sense of section (2.2.4).

To observe anelastic behaviour an internal variable is needed, and this variable must lag behind the applied strain as in equation (2.15). In this equation it was assumed the existence of an internal variable ξ coupled to the stress on the sample, and whenever a stress was applied, the variable ξ didn't take the equilibrium value $\bar{\xi}$ but instead varied as in equation (2.15). Such lagging can be caused by impurities, or by potential energy barriers as those described by the Peierls Nabarro Model (see section 3.1.2).

The presence of barriers to the movement of dislocations produces relaxation effects, such as those studied in section 2.2.3. These relaxation effects create peaks in the internal friction versus temperature graphs (recall that in section 2.2.5 the temperature was connected to the natural frequency of the system). Of the many internal friction peaks that have been observed in solids, one that has attracted the most attention is the Bordoni peak. This peak was found for the first time by Bordoni [15], [16] in 1949, and in the subsequent years this relaxation process was characterized experimentally. Most of the evidence indicates that the relaxation process of the Bordoni peak involves dislocations, although the exact mechanism has not been found yet. In other types of crystals similar type of peaks appear which are analogous to the Bordoni peak [5], [6] but the exact mechanism is not known either.

In this chapter we will first review the characteristics of the Bordoni peak and then the theory to explain this phenomenon that has been advanced so far, will be studied.

4.1 Characteristics of the Bordoni Peak

In the original work of Bordoni [15], he found that in Cu, Ag, Pb and Al a peak in the internal friction appeared around 10 KHz in the range of 50 K to 100 K (about one third of the Debye temperature). It was later found that the peak was essentially independent of the strain amplitud for small values of the strain [17], [4].

The main features of the peak taken mainly from [4], [16] and [3] are as follows:

1. The peak occurs in both single crystals and polycrystals. It appears in all FCC crystals.
2. The height of the peak increases with the amount of cold working and the maximum of the peak shifts to higher temperatures with more plastic deformation. The effects saturate at 2% to 3% of plastic strain.
3. The peak disappears after annealing at high temperatures.
4. Impurities reduce the height of the peak, neutron radiation causes the same effect.
5. In addition to the main peak there is a subsidiary peak observed at lower temperature. This peak is usually called the Niblett and Wilks peak and its size is always proportional to the Bordoni Peak. [17]
6. The temperature of the peak, that is, the temperature at which Q^{-1} has a maximum depends on the frequency of the wave: If the frequency grows the temperature at which the peak is found also grows.
7. The peaks show an Arrhenius dependence in temperature as in equation (2.16) but they cannot be described by a single relaxation process.

Many of the characteristics listed suggest that the peak is due to dislocations. The fact that the height of the peak increases with increasing cold working is one of these. Cold working corresponds to applying deformations on a sample to produce more dislocations in the sample, the dislocation density in the sample increases when the crystal is subject to more cold working. Impurities and neutron radiation may lower the peak height because they pin the dislocation down which restricts their movement and thus lowers the amplitude of the peak. Experimental curves for copper are shown in figure 4.1.

4.2 Seeger's theory of the Bordoni Peak

Seeger published a theory explaining the observations of Bordoni and of Niblett and Wilks in 1956 [18]. From the characteristics of the peak he concluded that the peak was related to the intrinsic properties of dislocations. He considers a crystal with a periodic potential similar to the potential calculated int he Peierls Nabarro model. In figure 4.2 the potential is depicted schematically with a period a, This period will naturally be related to the Burgers vector. The minimum shear stress τ_p necessary to take the dislocation from one minimum to the other is the Peierls stress.

As has been noted by Mott and Nabarro [19], dislocations at non zero temperature form kinks, see 4.3. Both the energy and entropy of the system increase in the presence of a kink.

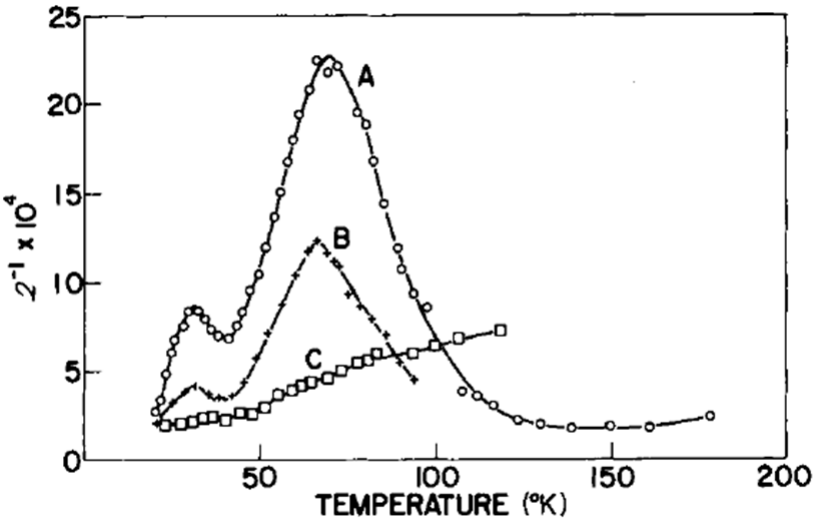

Figure 4.1: Internal friction vs temperature in three different copper samples. (a) Sample after a deformation of 8.4%. (b) Sample annealed for an hour at 180°C. (c) Sample annealed for an hour at 340°C.

If we call W_k the kink energy which is the energy needed to move a piece of the dislocation from one minimum to the other then, in thermal equilibrium, the number of kinks per unit length will be proportional to $e^{-\frac{W_k}{kT}}$. If a shear stress tends to move the dislocation in the y direction, then the distribution of kinks will change, new kinks will appear because of thermally activated processes and a relaxation phenomenon will appear if the shear stress is oscillatory. Seeger concluded that a peak will appear when the frequency of the applied stress f is equal to the frequency of formation of kink-antikink pairs ν. The kink-antikink pairs can be seen in figure 4.3.

Seeger described the dynamics of a dislocation considering it as a continuous function $y(x)$, which represents the relative displacement of atoms facing each other on opposite sides of the glide plane (dislocation line), see figure 4.3. The quantitative theory of Seeger starts by treating the dislocation line as a string parallel to the x axis with mass m per unit length and subject to an effective potential $E(y)$:

$$E(y)\frac{\mathrm{d}^2y}{\mathrm{d}x^2} = \frac{\mathrm{d}E}{\mathrm{d}y} - b\tau + m\frac{\partial^2 y}{\partial t^2} \tag{4.1}$$

The term on the left corresponds to the force related to the curvature of the string, the first term on the right is the force on the dislocation due to the periodic potential and the second term on the right is the force on the dislocation due to the shear stress. $E(y)$ is considered as a periodic function of period a, and can be approximated expressing the function as the first two terms of a Fourier series:

$$E(y) = E_0 - \alpha_1 \cos\frac{2\pi y}{a} - \alpha_2 \cos\frac{4\pi y}{a} \tag{4.2}$$

Notice that this expression is very similar to the Peierls Nabarro potential in equation (3.16), this similarity will be relevant later. Seeger assumes furthermore that E_0 is bigger than α_1 or

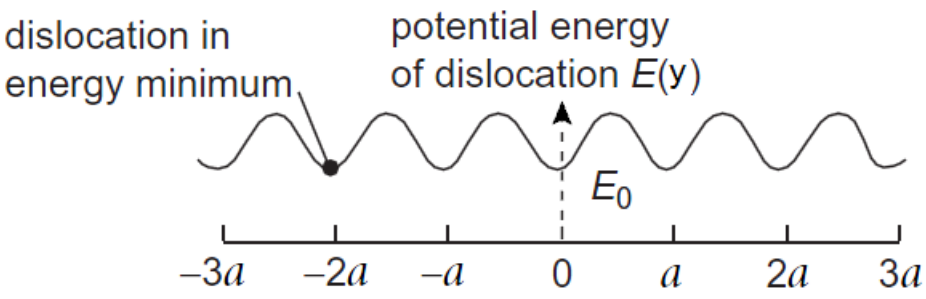

Figure 4.2: Illustration of the potential energy to which the dislocation is subject to. The periodicity of the potential a is the lattice constant. The difference between the maximum and the minimum is the Peierls stress (Figure modified from [10]).

α_2, then $E(y)$ on the left side of equation (4.1) can be replaced by E_0. For a time independent treatment of the problem the ordinary differential equation (ODE) obtained becomes

$$E_0 \frac{\mathrm{d}^2 y}{\mathrm{d}x^2} = \frac{2\pi\alpha_1}{a}(\sin\frac{2\pi y}{a} + 2\gamma \sin\frac{4\pi y}{a}) - b\tau \tag{4.3}$$

where $\gamma = \frac{\alpha_2}{\alpha_1}$. One solution of this ODE is a single kink, whose analytic form is [18]

$$y(x) = \frac{a}{\pi}\tan^{-1}\left(\frac{(1+4\gamma)^{\frac{1}{2}}}{\sinh[\frac{2\pi x}{a}\Omega]}\right) \tag{4.4}$$

with $\Omega = (\frac{\alpha_1(1+4\gamma)}{E_0})^{\frac{1}{2}}$. If we consider $\gamma = 0$, which implies $\alpha_2 = 0$, then equation (4.2) has the form of the energy obtained in the Peierls Nabarro model, for example compare with equation (3.16). In this case the kink becomes

$$y(x) = \frac{2a}{\pi}\tan^{-1}\left[\exp\frac{2\pi x}{a}\left(\frac{\alpha_1}{E_0}\right)^{\frac{1}{2}}\right]. \tag{4.5}$$

The kink width is defined as $w = \frac{1}{2}a\left(\frac{E_0}{\alpha_1}\right)^{1/2}$. Inserting (4.5) in

$$E_{pot} = \int_{-\infty}^{\infty} \frac{1}{2}E_0\left(\frac{\mathrm{d}y}{\mathrm{d}x}\right)^2 + \alpha_1\left(1-\cos(2\pi y/a)\right)$$

and identifying the potential energy of the kink configuration as W_k, we obtain

$$W_k = \frac{2a}{\pi}\left(\frac{2E_0 ab\tau_p}{\pi}\right)^{1/2}, \tag{4.6}$$

with

$$\tau_p = \frac{2\pi\alpha_1}{ab}. \tag{4.7}$$

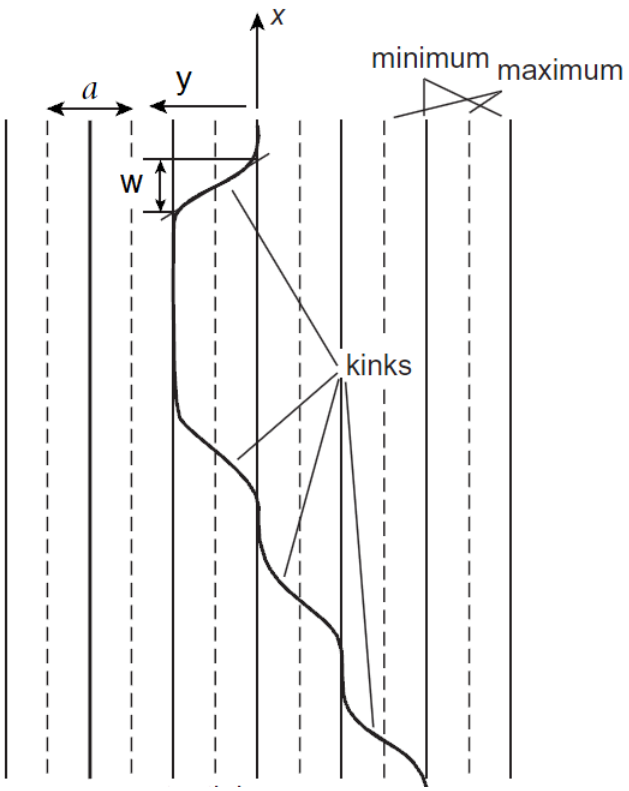

Figure 4.3: A dislocation line $y(x)$ in a periodic potential as imagined by Seeger. w is the width of the kinks and a the lattice constant (Figure modified from [10]).

Equation (4.7) comes from comparing equation (4.9) with (3.16) and (3.17), and considering $\alpha_2 = 0$.

There is one last modification that Seeger did to the calculation of W_k in his original article. Once the two kinks are created they will interact. Consider for example figure 4.3, in this configuration a pair of kinks will attract each other because of the direction of the Burgers vectors. If there is no applied shear stress it is then expected that these kinks will move towards each other and annihilate. If on the other hand there is a shear stress τ applied, there will exist a critical distance d_{cr} in which if $\mathrm{d} < \mathrm{d}_{cr}$ where d is the distance between the kinks, then the kinks will annihilate. Otherwise they will separate further until they don't interact. This critical distance will depend on the applied shear stress. Because of the critical distance explained above, the activation energy of the kink W_k will also depend on d_{cr}. The effect of the critical distance will manifest as a logarithmic dependence of W_k on τ. This dependence is very small for experimental detection and aside from this effect the Bordoni Peak is independent of the amplitude. The detail of the calculation is in Seeger's article [18], here we cite the result to show the logarithmic dependence of W on τ:

$$W = W_k \left[1 + \frac{1}{4} \log \left(\frac{16\tau_p}{\pi\tau} \right) \right] \tag{4.8}$$

4.2.1 Connection of Seeger's theory with experiment

At the time of Seeger's work, the experiments of internal friction were done using a torsion pendulum at a fixed frequency and varying the temperature, the curves obtained are shown in 4.1. Since the frequency of the oscillations was fixed, the parameter varied was the relaxation time τ which depends on temperature according to equation 2.17. Recall that in the equation that relates τ and temperature there is the parameter Q, the activation energy of the relaxation process which coincides with W calculated in this section. In this way it is possible to fit this Lorentzian function to the experiment and obtain an experimental value of the activation energy. Seeger assumed that the frequency of kink formation has the simple form

$$\nu = \nu_0 \mathrm{e}^{-W/kT} \tag{4.9}$$

where ν_0 is a frequency independent of temperature and W is the activation energy of the process. In equation (2.17) there is also a τ_0 that is related to ν_0 in equation (4.9). To relate the experimental value with the parameters of the model it is assumed that ν_0 is the natural frequency of rigid dislocation line in the minimum of the potential, then

$$\nu_0 = \frac{v_t}{a}\left[\frac{(1+4\gamma)\alpha_1}{E_0}\right]^{\frac{1}{2}} \tag{4.10}$$

where v_t is the velocity of shear waves; also, in the article [18] it is considered that $E_0 = \frac{1}{5}Gb^2$.

As was mentioned at the beginning of this section, along with the Bordoni Peak there is a smaller peak at lower temperatures called the Niblet-Wilks peak. Seeger ascribed this smaller peak observed originally in copper to the different directions of dislocation in the sample. In FCC crystals the typical dislocation has a Burgers vector in the directions $\langle 110 \rangle$, this is the close packing direction in this type of crystal. The direction of these dislocations lie in the $\{111\}$ glide plane, and they can be parallel or form an angle of $\pm 60^\circ$ thus the different peaks are due to these two types of dislocations. Seeger's explanation for the appearance of the two peaks is that since the activation energy of the two types of dislocation differ by two orders of magnitude, then these difference in activation energies cause two different relaxation peaks.

4.3 Bordoni Peak and experiments

Interpreting measurements in FCC crystals of the Peierls stress σ_p has been hard because of the different methods used: One way for estimating σ_p is by resolving the critical resolved shear stress measured by mechanical deformation test [20],[1] which consists in measuring the shear stress required to initiate plastic deformation. Other way is through the Bordoni peak relaxation. It is possible to calculate as explained in the last section σ_p from the relaxation measurements. Mechanical deformation tests give a Peierls stress in the range of $10^{-4}G$ to $10^{-5}G$ and Bordoni peak relaxations give an estimation from $10^{-2}G$ to $10^{-3}G$, where G is the shear modulus of the material. This discrepancy of two orders of magnitude has been the origin of the questioning of the kink pair formation origin of the Bordoni peak [21]. This thesis attempts to shed light on these issues through direct numerical simulations. Such is the subject of the next chapter.

Chapter 5

Molecular Dynamics simulation

Now that the context of this thesis has been laid, the new numerical work that has been performed will be described. As was mentioned in section 4.3 there is confusion on the interpretation of the experimental data obtained through the Bordoni peak: it is not clear yet what is the microscopic mechanism responsible for this effect and the objective of this simulations are to shed light on this mechanism.

Nowadays the main experimental tool used to probe the microscopic properties of dislocations is the transmission electron microscopy (TEM). On the other hand, the main theoretical tool for studying dislocations is continuum mechanics. There is then the need to connect the atomic scale measurements of dislocations (and in particular measurements of the Bordoni peak) and continuum mechanics predictions which correspond to the scale of the hundreds of atoms and higher.

Recent advances in the study of dislocation dynamics [22], [23], [24] and the study of dislocations through ultrasound measurements increase the need to connect measurements and theory, and the most natural candidate is numerical simulations. The origin of the Bordoni peak seems to be connected to the intrinsic properties of dislocations, as has been mentioned before, thus simulations of this phenomenon is interesting for these purposes.

Recent simulations are relevant for the work done in this thesis. In a work done by Marian and Caro [25], the dynamics of dislocations was studied using molecular dynamics (MD) simulations of Ni-Au alloys. The mobility of dislocations in Ni with different Au concentrations was measured. A measurement of interest was the velocity of the dislocation as a function of the stress applied on the sample, similar measurements were made in this thesis in Cu and Ni. Also the work of Skirlo and Demkowitz [26] is relevant, they found viscoelastic effects in super-lattices of Cu-Nb. This viscoelastic effect is found by applying oscillatory shear stresses on the sample in a similar way done in this thesis. They found a hysteresis loop similar to the one that may be expected from the anelastic relaxation of the Bordoni Peak.

For the reasons exposed before it is interesting to go beyond the analytical models and understand through simulations the microscopic dynamics of an FCC metal (in these type

of crystals is where the Bordoni peak is found) that is forced with an oscillatory shear strain mimicking the experiments done in the last century.

In this chapter it is proposed to study the Bordoni peak through molecular dynamics simulations in FCC crystals. For this purpose the LAMMPS molecular dynamics simulator [27] was used and for visualization of the samples the OVITO software [28] will be used.

In order to obtain the Bordoni peak through simulations, first samples of FCC crystals were created with two edge dislocations which formed four partial dislocations in total. The reason for the two dislocations instead of one was that simulations with one dislocation resulted in image effects, which caused stresses over the single dislocation. Two edge dislocations on the other hand achieved an equilibrium position, with the dislocations at 45°. Analytical calculations of the internal friction were made considering the dislocation as an overdamped string. This calculations were done in order to interpret the measurements of internal friction and also to have an estimation of the orders in magnitude involved in the simulations. Once the internal friction was estimated the samples were subject to oscillatory shear strains at different temperatures and the stress and the strain in the sample were measured. By plotting stress vs strain, it is expected to obtain a hysteresis loop corresponding to the anelastic relaxation

The samples used were copper and nickel crystals with 892 800 atoms. EAM (Embedded atom model) potentials ([29], [30]) were used for the simulations. The potential for copper can be found in [31] and the nickel potential can be found in [32], both of which can be downloaded from the Interatomic potentials repository [33]. Only results for copper are reported here. The Ni results are not reported since there were some problems with the calculation of the line tension of the dislocations in Ni.

5.1 Preparation of samples

Two FCC crystal samples of copper and nickel were prepared, each crystal type is composed of 892 800 atoms. Both crystals have approximate x,y and z dimensions 240 Å $\times$ 200 Å $\times$ 200 Å respectively (see figure 5.1). The boundaries in the x direction are free; later, velocities will be imposed to them. In the y and z direction the boundary conditions are periodic. First the copper crystal was created and then the positions of the atoms were scaled considering the lattice distance of nickel in order to create this type of crystal.

To create in the sample an edge dislocation, three contiguous half planes parallel to the normal of the $\{111\}$ plane were erased. This procedure was done two times to give two edge dislocations with the corresponding slip plane $\{111\}$. After erasing the half planes, the sample was thermalized at $T = 0$ K with the NVT ensemble, the partial dislocations and the stacking fault appear spontanously. Each dislocation is composed of two partial dislocations joined by a stacking fault whose size is determined by the interaction between the partial dislocations. This partial dislocations in FCC crystals are called Shockley partials [10]. See appendix B. The Burgers vector of the original dislocations is in the direction $\langle 110 \rangle$, the x direction in the sample. Note that the sample used has dislocations with Burgers vector

in very specific directions, in a real sample it will be true that dislocations will have many different directions, which may or may not separate into partials. This will be mean that when comparing results of internal friction in our simulations and experiments, it must be considered that the dislocations present in experimental set ups with different directions will increase the internal friction. Finally, note that the sample has a dislocation density of approximately 10^{-4} Å^{-2}, this is a very high dislocation density compared to metals used in everyday applications [10] but as explained later, it is a density achievable experimentally.

The reason for creating two dislocations is that when the samples contained one dislocation, image stresses appeared because of the free faces in the x direction. The disposition of the dislocations in the samples is shown in figure 5.1, with the x,y and z axes defined. The system with the atom positions was prepared by Enrique Martinez from Los Alamos National Laboratory. A velocity distribution was given to the atoms with the velocity command of LAMMPS. The samples were initially prepared at $T = 0.0001$ K with this command.

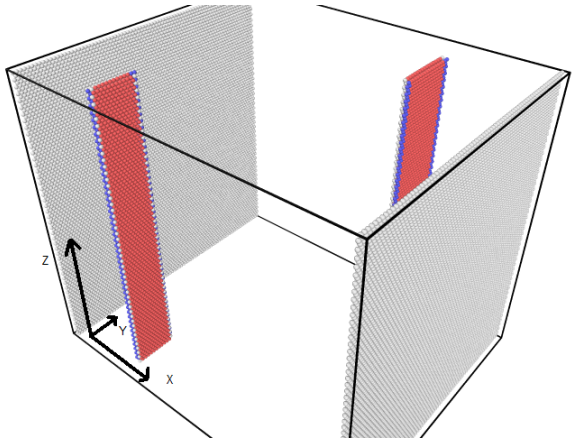

Figure 5.1: Sample of Cu created with 2 dislocations. The blue atoms are in BCC order, the red atoms are HCP and gray is unknown (not BCC, FCC or HCP), FCC atoms have been removed for visualization. Red atoms correspond to the stacking fault between the partial dislocations. The figure corresponds to 892800 atoms, and approximate x, y and z dimensions 240 Å$\times$200 Å$\times$200 Å, respectively. Notice that the dislocations have dissociated into partial dislocations. The distance between these partial dislocation is 12 atomic distances.

5.2 Finding hysteresis in Cu

To look for hysteresis in Cu, the samples described in section 5.1 were heated to 50 K, 100 K, 150 K, 200 K and 250 K. Also simulations at 0 K temperature were done where it was observed the kink-antikink pair formation applying a constant shear rate to the pinned dislocation, see figure 5.2 for an image. This heating was done in 300 000 time steps with $\Delta t = 0.002$ ps. The temperature was changed by using the temperature rescaling algorithm of LAMMPS which rescales the particle velocities until the desired temperature was obtained. After heating, each sample was thermalized for 50 000 steps with the NVT integrator of LAMMPS and using the fix temp/rescale command in LAMMPS. We note that the long time of thermalization was necesary so that the dislocations and the free boundaries of the

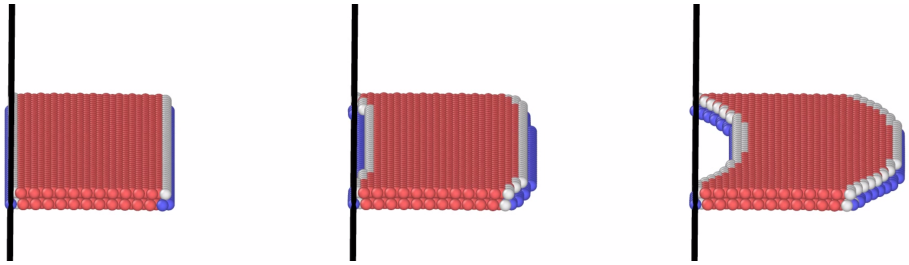

(a) (b) (c)

Figure 5.2: Kink pair formation at 0 K. The simulation was run with the dislocation pinned and a constant shear rate. It is possible to see the formation of the kink pairs and also the dislocation jumping from one minimum of the potential to the adjacent minimum. Shown in red are the HCP atoms, in blue the BCC atoms, and in white atoms in unknown order (FCC atoms have been erased for visualization).

surface stopped their oscillations caused by the change of temperature. To determine that the samples were thermalized, total energy of the system, the potential energy and the pressure were measured. In the thermalized state the total energy fluctuations and the potential energy fluctuations $\Delta E/E$ were of order 10^{-4}, in the case of pressure the fluctuations $\Delta P/P$ were of order 1/40. The size of pressure fluctuations in MD simulations is normally bigger than other variables and has been reported in the LAMMPS manual. In the visualization of the sample the dislocations oscillate during the thermalization and when the criteria are fulfilled the oscillations cease.

Once the samples at different temperatures were at thermal equilibrium, the dislocations were pinned at the top and the bottom. Two methods were used to pin the dislocations: one was to take spheres with a radius of 15 Å in the extremes of the dislocations and imposing that any external force imparted to the atoms inside the sphere be zero. Note that the atoms outside the sphere would still feel the potential from the atoms inside the sphere. A second method was to erase the atoms inside the spheres within a radius of 15 Å. The empty spheres form vacancies in the system that pin the dislocations. The first method was chosen over the second because the vacancies introduce unknown interactions with the dislocation that may affect the measurements of internal friction.

After thermalizing and pinning the dislocations, the thermostat in the sample was turned off so that the dissipated energy could be measured and they were subject to oscillatory shear strains. This shear strains were applied by imposing the trajectory $x(t) = x_0 + A\sin(\frac{2\pi}{T}t)$ on all the atoms in the free walls of the crystal, where x_0 is the initial position of the atom in the free wall, T is the period and A the amplitude. The amplitude used for copper and nickel was 1 Å. The period used initially was 125 ps. This period was chosen after a trial and error test so that the length of one cycle in the simulation took a reasonable time (see the Appendix for the simulation times). The amplitude was chosen such that $\mathrm{d}x/\mathrm{d}t$ was not greater than one half the speed of sound in Cu. The stress on the sample was measured using the LAMMPS command that computes the stress per atom in the sample and then it was averaged over all the atoms. The stress and strain plots are show in figure 5.3.

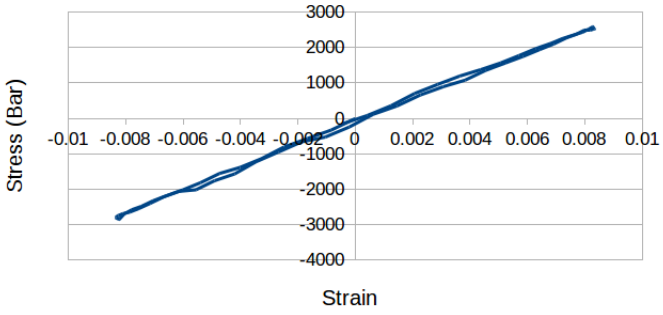

(a) Temperature = 50 K, Period = 125 ps

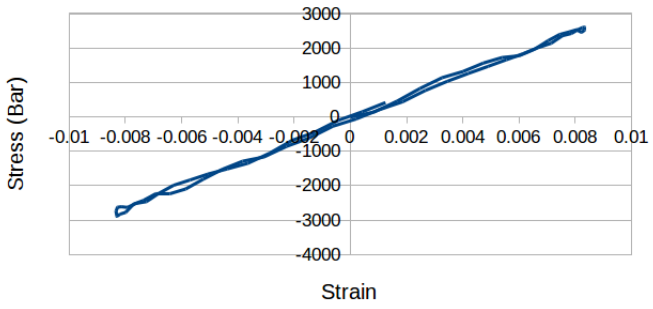

(b) Temperature = 100 K, Period = 125 ps

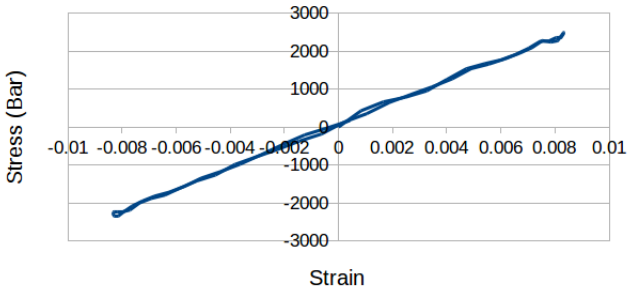

(c) Temperature = 150 K, Period = 125 ps

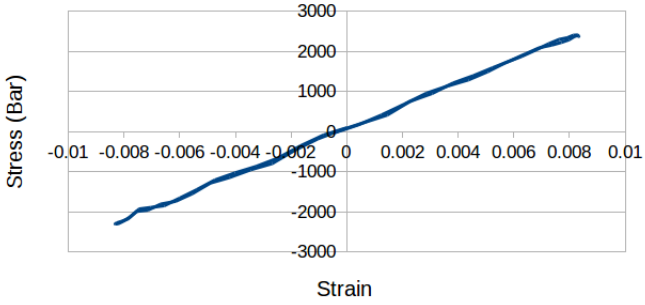

(d) Temperature = 200 K, Period = 125 ps

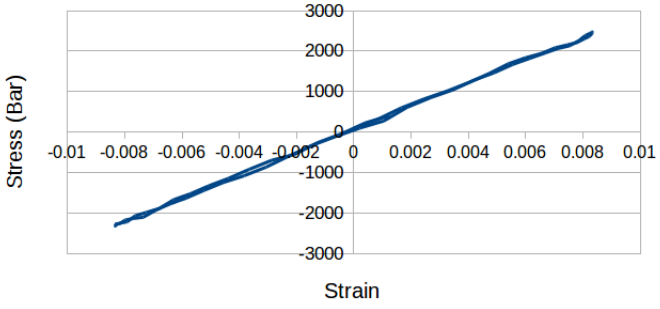

(e) Temperature = 250 K, Period = 125 ps

Figure 5.3: Stress σ_{xy} v/s Strain ε_{xy} plot. The graph were produced by applying an oscillatory strain on the sample with a period of 125 ps and amplitude 0.008. An oscillatory trajectory is given to the atoms in the free wall to impose an oscillatory shear strain. The amplitude of the oscillation is 1 Å. The plot was created by running the simulation by 5 cycles and averaging over the last three cycles the σ_{xy} component of the stress tensor. The points where sampled every 1000 timesteps giving 64 points for each plot.

5.3 Estimation of internal friction

After the initial simulation carried out with a period determined by trial and error, an analytical calculation was performed to determine the ideal period. In order to estimate the internal friction we must remember the formula (2.7). This formula relates the dissipated energy in a cycle and the maximum stored energy with the internal friction. In this formula the internal friction is defined as $Q^{-1} = \tan\phi$ where ϕ is the phase lag of the strain with respect to the stress. To estimate this quantity we need to calculate the dissipated energy in the sample in one cycle, called ΔW, and the maximum stored energy W.

5.3.1 Estimation of ΔW

For the calculation of the dissipated energy in one cycle the dislocation will be approximated with the equation of the overdamped string that is externally loaded with a periodic forcing. The equation used comes from the string model used in [22], where the equation given is

$$m\ddot{x} + \gamma\dot{x}(s,t) - \Gamma x''(s,t) = F_{PK}. \tag{5.1}$$

where γ is the damping coefficient, Γ is the line tension and $F_{PK} = \sigma b$ is called the Peach Koehler force per unit length, σ is the stress on the dislocation and b is the Burgers vector

The first researchers to approximate dislocations as continuous strings and relate this to internal friction were Granato and Lucke [34], [35]. Here we will follow a similar approximation. We assume a periodic force on the string which has pinned endpoints $x(0,t) = x(L,t) = 0$. The loading frequencies are low enough that inertia terms are negligible. The starting point is the equation

$$\gamma\dot{x}(s,t) - \Gamma x''(s,t) = Fsen(\omega t). \tag{5.2}$$

with F the maximum force per unit length and the mass term is neglected. We assume $x(s,t) = x(t)sin(\pi s/L)$ since at low frequencies only the fundamental mode of the string will be excited. Note that this is not the solution of 5.2, at $s = 0, L$. This assumption should instead be regarded as a variational ansatz to equation 5.2 the equation is no satisfied and then the equation is integrated $\frac{1}{L}\int_0^L$, it is thus obtained

$$\gamma\dot{x} + \Gamma(\frac{\pi}{L})^2 x = \frac{\pi}{2}Fsen(\omega t)$$

The homogeneous solution to this equation is;

$$x(t) = x_0 \mathrm{e}^{-\frac{t}{\tau}}, \tag{5.3}$$

where $\tau^{-1} = \frac{\Gamma}{\gamma}(\frac{\pi}{L})^2$ defines a relaxation time. The particular solution to the inhomogeneous equation is obtained by considering

$$x(t) = \alpha cos(\omega t) + \beta sin(\omega t).$$

Inserting this in (5.2) we obtain

$$\gamma\tau^{-1}(\alpha^2 + \beta^2) = \frac{\pi}{2}F\beta, \tag{5.4}$$

$$-(\alpha^2+\beta^2)\gamma\omega = \frac{\pi}{2}F\alpha. \tag{5.5}$$

If we make the change of variables $\alpha = Acos(\phi)$ and $\beta = Asen(\phi)$, and then divide equation (5.4) by equation (5.5) we obtain

$$\frac{\tau^{-1}}{\omega} = tan(\phi).$$

Maximum hysteresis is obtained when $\phi = \frac{\pi}{4}$, the verification of this is mentioned later. Then

$$\omega = \tau^{-1} = \frac{\Gamma}{\gamma}(\frac{\pi}{L})^2. \tag{5.6}$$

This defines the applied frequency at which we expect maximum losses. Notice that using a continuum approximation we have found the optimal frequency of the forcing to get the maximum dissipation of energy. We must now relate this ω to the parameters L, Γ and γ of our numerical sample.

In order to determine γ we proceed as follows: we let the dislocation free, i.e. without pinning at the ends, and apply a constant and uniform stress to the sample. In this case equation (5.2) indicates that the dislocation will acquire a constant velocity proportional to the stress, with a constant of proportionality determined by γ. Thus, imposing an external strain and measuring the velocity imparted to the dislocation permits a determination of γ

These simulations were done for different shear strain rates and at a temperature of 0.0001 K. The obtained stresses are plotted against the corresponding dislocation velocities in figure 5.5. In this way the damping parameter can be calculated from the slope of the curve by the relation obtained later in equation (5.9) . To measure the stress in the sample, the compute stress/atom command from LAMMPS is used. This command calculates an average stress per atom on the sample when considering the whole sample.

In the simulations what is actually applied is a velocity to the walls as described in section 5.1, so it was necessary to calculate the dislocation velocity from the shear strain rate. This is possible from Orowan's law [10] which dictates

$$\frac{\mathrm{d}\varepsilon}{\mathrm{d}t} = \rho v_{\mathrm{d}} b. \tag{5.7}$$

where $\mathrm{d}\varepsilon/\mathrm{d}t$ is the strain rate, ρ is the dislocation density, v_{d} is the dislocation velocity and b is the Burgers vector.

Since in our copper sample there are two dislocations, equation (5.7) will take the form

$$v_{\mathrm{d}} = \frac{\mathrm{d}\varepsilon}{\mathrm{d}t}\frac{1}{\rho b} = \frac{\mathrm{d}x}{\mathrm{d}t}\frac{L_y}{2b}. \tag{5.8}$$

because $\frac{\mathrm{d}\varepsilon}{\mathrm{d}t} = \frac{\mathrm{d}x}{\mathrm{d}t}\frac{1}{L_x}$ and $\rho = \frac{2}{L_x L_y}$, where L_{i} is the length along the $\hat{\mathrm{i}}$ axis and x is the displacement of the walls in the $\hat{x}$ axis. The factor of 2 appears because there are two dislocations in the sample. Thus the relation between the dislocation velocity v_{d} and the velocity of the walls v is

$$v_{\mathrm{d}} = v\frac{L}{b}$$

Finally γ is given by $\gamma = F_{PK}/v_{\mathrm{d}}$, where F_{PK} is the Peach Koehler force per unit length which is given by $F_{PK} = \sigma b$ and the slope p of the graph σ vs v is $p = \frac{\sigma}{v}$, where v is the speed of the free walls. In conclusion we have

$$\gamma = p\frac{b^2}{L} = \frac{\sigma b}{v_{\mathrm{d}}}. \tag{5.9}$$

This determines γ in terms of slope p, Burgers vector b and dislocation velocity v_{d}.

Figure 5.5 shows the stress of the sample as a function of time for several different, applied strains to the walls of the sample. After a transient, a regime of constant (on average) shear stress is established. This measured average stress is plotted against the wall velocity v, which is given in terms of the applied strain rate by equation (5.7), in figure 5.4 the six red points were used to infer an average slope. The value for γ obtained is

$$\gamma = 1406.25 \pm 35.3 \text{ Bars} \cdot \text{ps}$$

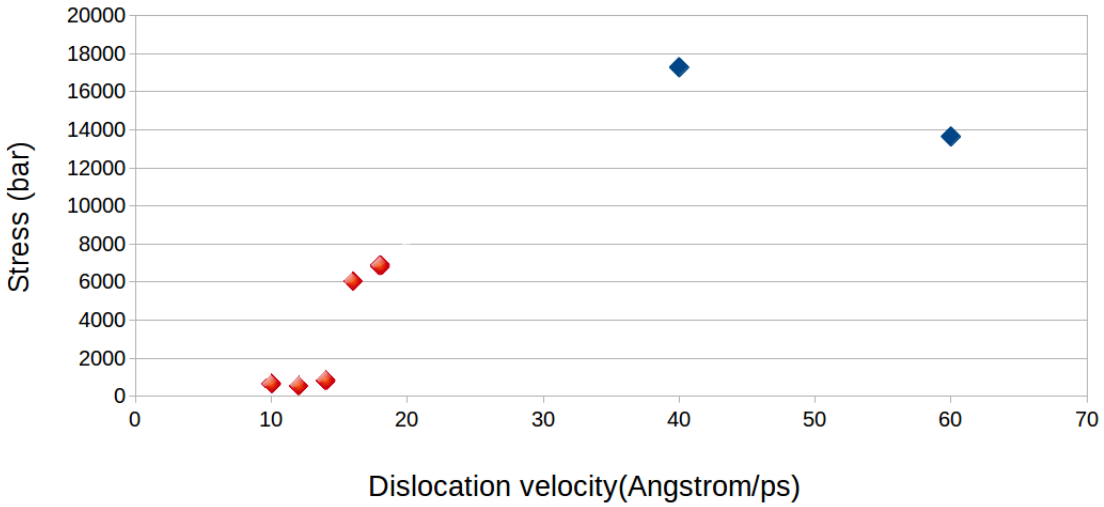

Figure 5.4: Stress vs dislocation velocity in Cu plot. A constant shear strain rate was applied to the Cu sample, which gives the dislocation a constant velocity. The stress is measured and then plotted. The six red points were used to infer an averged slope of $p = 45000$ Bars$\cdot$ps/Å. The values over 0.2 Å/ps were not considered for the calculation of γ because the speed of the dislocation is 20 Å/ps, about the speed of sound in Copper.

In order to calculate Γ a simulation with no dislocations and periodic boundary conditions was run, and then the total energy was calculated. The difference of the total energy with dislocations and without dislocations divided by the length of the two dislocations gives Γ. The energy of the sample without dislocations was calculated by multiplying the cohesion energy given by the potential [31] by the total number of atoms. To check that the given cohesion energy was correct, a simulation with no dislocations was run and the total energy was found to be the cohesion energy multiplied by the number of atoms in the sample

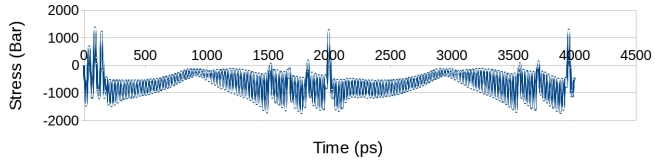

(a) Dislocation velocity 10 Å/ps

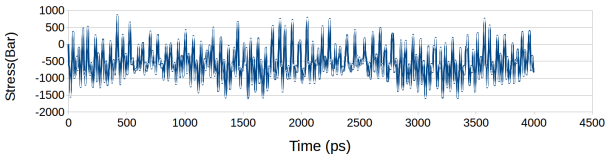

(b) Dislocation velocity 12 Å/ps

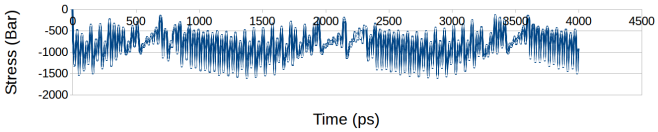

(c) Dislocation velocity 14 Å/ps

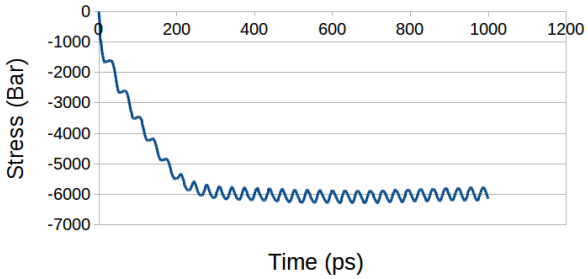

(d) Dislocation velocity 16 Å/ps

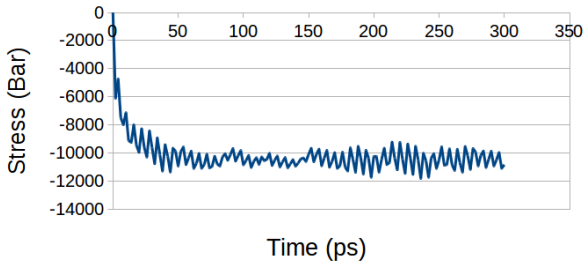

(e) Dislocation velocity 18 Å/ps

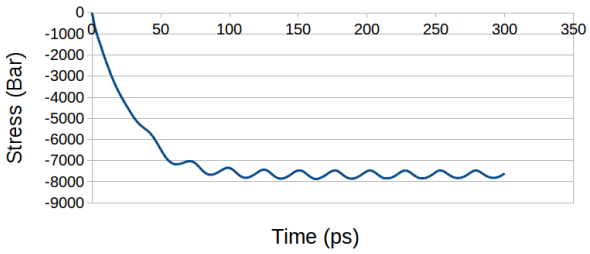

(f) Dislocation velocity 20 Å/ps

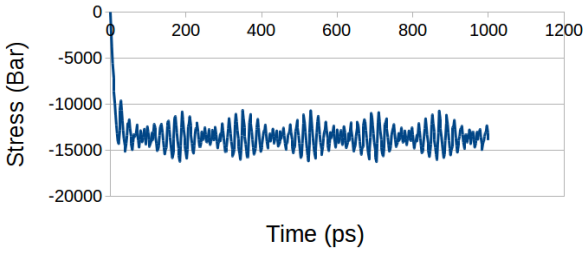

(g) Dislocation velocity 60 Å/ps

Figure 5.5: Stress σ_{xy} vs time of the simulation in the Cu sample. Graph was produced by applying a constant shear strain rate on a sample with unpinned dislocations, after a time depending on the shear rate the stress takes an average equilibrium value. The sample was at a temperature of 0.0001 K. Notice the difference in the plots for speeds higher than 16 Å/ps and those lower than this speed. It is unclear the origin for the difference between these speeds.

without dislocations, the cohesion energy given by the potential and the one calculated from the sample were equal to -3.54 eV/ Å. The temperature of all the simulations mentioned above was 0.0001 K.

The results for the parameters mentioned in the case of copper were

$$\Gamma = 1.225 \text{ eV/Å}$$
$$L = 200 \text{ Å}$$
$$b = 2.2 \text{ Å}$$
$$p = 45000 \pm 1460 \text{ Bars} \cdot \text{ps/Å}$$
$$\gamma = 1406.25 \pm 35.3 \text{ Bars} \cdot \text{ps}$$

Using these values in equation 5.6 we obtain the period at which we expect maximum damping between dislocation motion and applied load. Note that the dissipation in the maximum of hysteresis depends on γ. If we assume the dislocation is a string, then the equation for the energy dissipated in a cycle are the same as the equation of a damped oscillator. In the case of the damped oscillator as the damping increases so does the maximum dissipation; the same is expected for this case.

With γ and Γ it was possible to check if the assumption of disregarding the inertial term in equation 5.1 was true. For this we compare the terms $m\frac{4\pi^2 A}{T^2}$, $\gamma\frac{2\pi A}{T}$ and $\Gamma\frac{\pi^2 A}{L^2}$ where A is the amplitude of the trajectory and m is the mass per unit length of the dislocation. This mass per unit length is defined as [22]

$$m \simeq \frac{\rho b^2}{4\pi}$$

with ρ the density of copper and b the Burgers vector of the dislocation. Taking the value of the density as $\rho = 8.96\text{g/cm}^3$ and $b = 2.2$ Å we obtain

$$m\ddot{x} \sim m\frac{4\pi^2 A}{T^2} = 1.2 \times 10^4 \text{ J /m}^2$$

$$\gamma\dot{x} \sim \gamma\frac{2\pi A}{T} = 2.3 \times 10^8 \text{ J /m}^2$$

$$-\Gamma x'' \sim \Gamma\frac{\pi^2 A}{L^2} = 9.6 \times 10^9 \text{ J /m}^2$$

This confirms that the approximation done is consistent. With all these data and the discussion above we can calculate the frequency at which the hysteresis is maximum and the corresponding period.

$$\omega_{max} = 0.165 \pm 0.0004 \times 10^{12} \text{ rad/s} \tag{5.10}$$

$$T_{max} = \frac{2\pi}{\omega} = 38 \pm 0.0002 \text{ ps} \tag{5.11}$$

With the values of the parameters obtained, a numerical model of equation (5.2) was set up in Mathematica. The equation was solved and the functions $x(t)$ and $F\sin(\omega t)$ were obtained

(notice that F depends on ϕ). For the amplitude of the force, the value of the stress in a sample subject to shear strain was measured, the maximum value of the stress corresponding to the maximum displacement of the free boundary of the sample was used. The solutions are plotted in figure 5.6.

In order to calculate ΔW, the area of the resulting ellipse is measured (see figure 5.7). The result of this area for copper was

$$\Delta W = 2.88 \times 10^{-2} \text{ eV} \tag{5.12}$$

This result was obtained by integrating the function in one cycle.

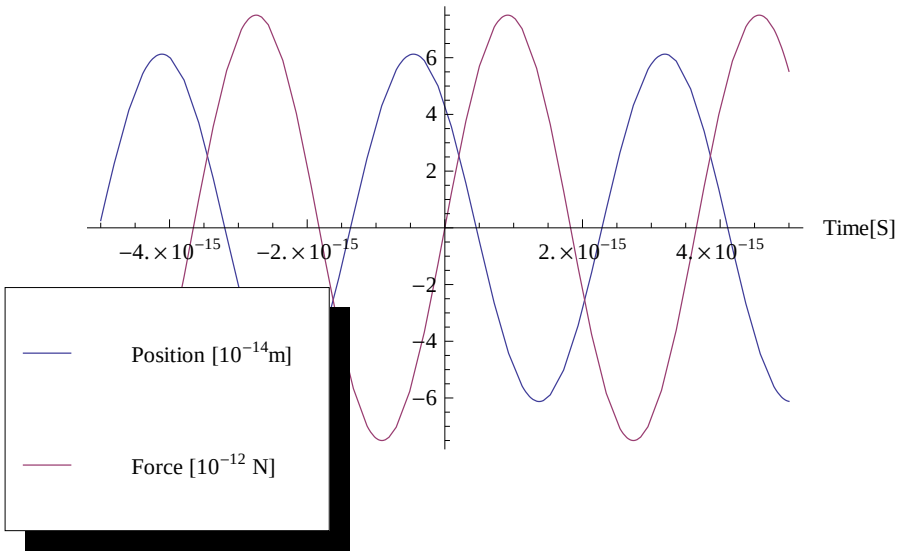

Figure 5.6: Force vs time and position vs time plot according to the solutions of equation 5.2. This graph corresponds to the force applied in the string model and to the position of the corrresponding oscillator. The model assumes the dislocation is an overdamped string. The parameters used were the ones calculated in section 5.3.1

5.3.2 Estimation of W

To estimate W, an oscillatory shear strain was imposed on the samples with a strain amplitude of 1 Å and a period of 38 ps (the period obtained in 5.11). The sample was at a temperature of 0.0001 K. From these simulations the total potential energy was calculated using the corresponding compute command of LAMMPS and plotted against time. These same simulations were done at 50 K and 100 K with very similar results. It is expected that this plot will indicate first the potential energy starts from a minimum and increases as the shear strain increases until it reaches a maximum and then decreases. This is expected because if the crystal is deformed from its equilibrium position, the total potential energy will increase. This increase in the potential energy is exactly the energy stored in the sample, thus if we substract the potential energy when there is no stress with the maximum of the

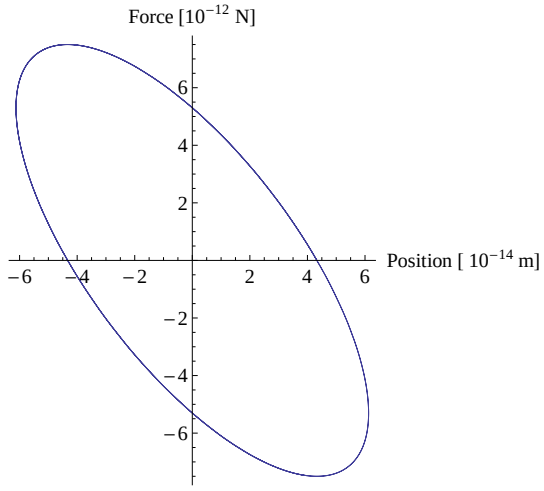

Figure 5.7: Force vs Position plot from equation 5.2. From the area of the hysteresis loop obtained it is possible to calculate ΔW.

potential energy in a cycle then we obtain the stored energy. Note that in these simulations it is needed that the dislocations remain pinned.

For copper we show the result of the simulation in figure 5.8. The values for the maximum and minimum were obtained by fitting a sine on the graph of figure 5.8. From this fitting, an error of ± 4.3eV was obtained. Subtracting both values gives the result $W = 35.2$ eV. LAMMPS computes with at least 12 significant figures so this difference is real.

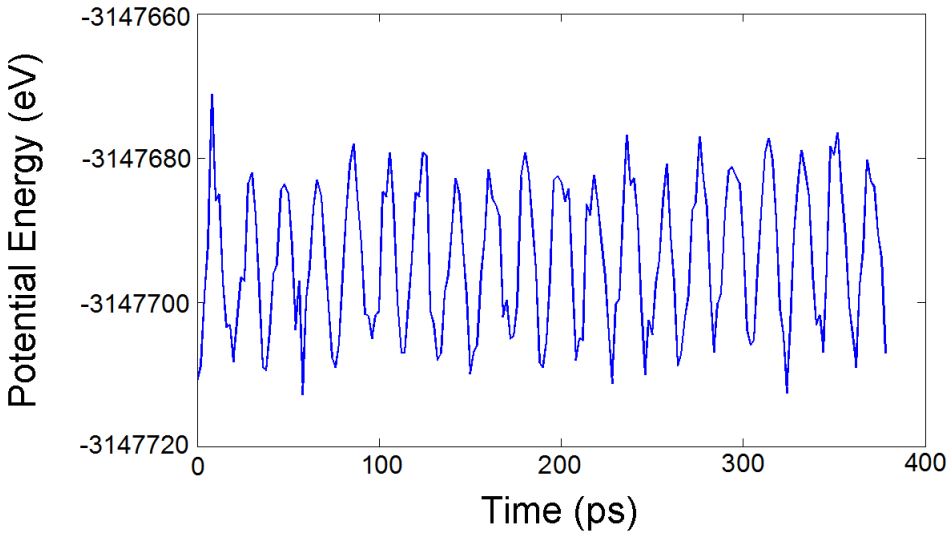

Figure 5.8: Potential energy of the sample vs the time of simulation in Cu. The sample was Cu at a temperature of 50 K, subject to an oscillatory strain by imposing an oscillatory trajectory on the boundary walls. The amplitude was of 1 Å and a period of 38 ps

.

5.3.3 Estimation of $\tan\phi$

With the calculation of W in section 5.3.2 and ΔW in section 5.3.1, the expected internal friction $\tan\phi = \frac{\Delta W}{2\pi W}$ was calculated.

For copper the result is

$$Q^{-1} = \tan\phi = 0.00012$$

This value is of the same order of magnitude to the one reported on experiments of internal friction on copper [36]. The low value for the hysteresis might be the reason that it is difficult to observe the hysteresis in the stress-strain plots, the phase difference between stress and strain will be approximately $\phi = 0.00012$. In the next section new molecular dynamics simulations will be done, and the curves will be integrated to compare their values of the area under the curve with the internal friction obtained in this section.

5.3.4 Limitations of estimation

One of the approximations for ΔW was to consider the dislocation as an overdamped string, this of course doesn't consider the discrete nature of the dislocation, it doesn't account for the partial dislocations and the stacking fault.

5.4 Simulation of internal friction

After the estimation through the analytical model, a fully atomistic calculation was performed. To this end an oscillatory stress was applied to the Cu and Ni samples. The samples used are the same as the ones described at the beginning of section 5.2. The period used for Cu in the oscillatory shear strain is the one shown in section 5.3.1, i.e. 38 ps. The stress-strain plots for Cu at temperatures 0 K, 50 K, 100 K, 150 K, 200 K and 250 K are shown in figure 5.9. These curves were obtained by performing 5 cycles and averaging over the last 3 cycles.

From the stress-strain plots, the area of the hysteresis loop was calculated. Note that these plots show stress v/s strain, if we want to compare with the area of hysteresis obtained in (5.12) we need to transform the units of the stress from bars to eV/ Å^3. The values of ΔW calculated for the simulation are summarized in table 5.1.

From the stress-strain plots it is possible to calculate the shear modulus. A line was fitted for each temperature and the error for the slope corresponds to the error in the calculated shear modulus. The results are shown in 5.10. The shear modulus of the copper sample without dislocations was also measured, the results are plotted in figure 5.11 and compared to experimental results from [37] where single copper crystals were used. The shear modulus as a function of temperature for samples with dislocation density similar to the sample in the simulations was not found in the literature. The dislocation density of the sample with dislocations is 5×10^{11} cm^{-2}. Nonetheless, the sample with dislocations was compared to

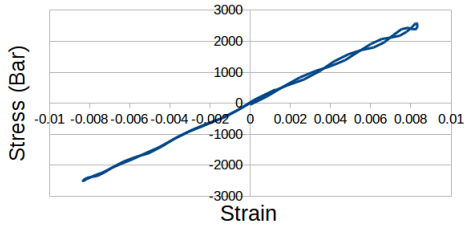

(a) Temperature = 0.0001 K, Period = 38 ps

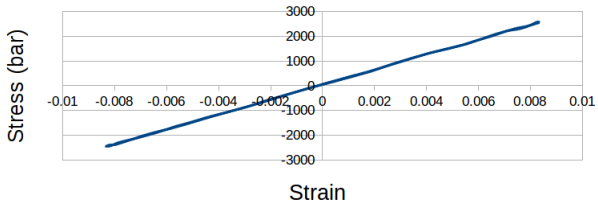

(b) Temperature = 50 K, Period = 38 ps

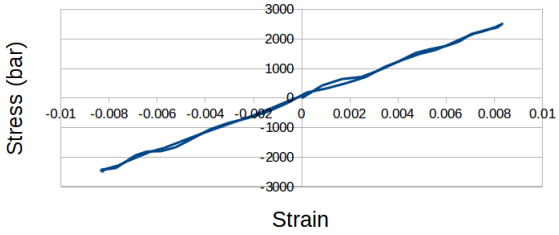

(c) Temperature = 100 K, Period = 38 ps

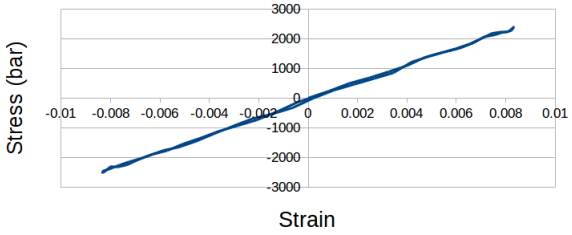

(d) Temperature = 150 K, Period = 38 ps

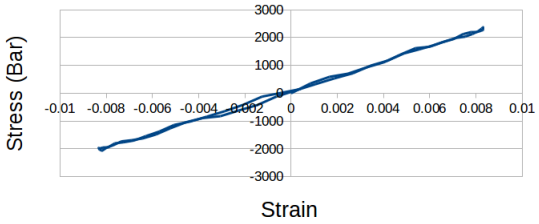

(e) Temperature = 200 K, Period = 38 ps

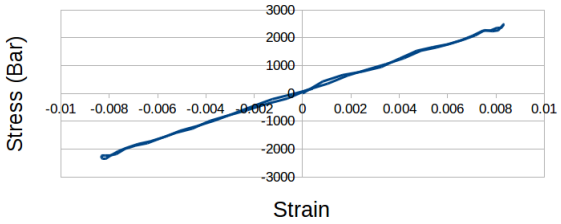

(f) Temperature = 250 K, Period = 38 ps

Figure 5.9: Stress σ_{xy} v/s Strain ε_{xy} plot. The graph was produced by applying an oscillatory strain on the sample with the period given by (5.11). An oscillatory trajectory is given to the atoms in the free wall to impose an oscillatory shear strain. The amplitude of the oscillation is 1 Å. The plot was created by running the simulation by 5 cycles and averaging over the last three cycles. The points where sampled every 1000 timesteps giving 64 points for each plot.

Temperature (K)	ΔW (eV)	Shear Modulus (GPa)
0	1.112	30.5
50	0.979	30.2
100	1.497	29.8
150	1.276	29.2
200	2.496	28.8
250	1.611	28.4

Table 5.1: Table with the results of the oscillatory stress simulations. ΔW was obtained by calculating the area of the hysteresis loop and the shear modulus by calculating the slope of a line fitted to the corresponding stress-strain plot. Compare with (5.12) which was calculated from the analytical model.

Temperature (K)	ΔW (eV)
0	-5.41×10^{-2}
50	1.3×10^{-2}
100	-1.2×10^{-2}
150	4.6×10^{-2}
200	-3.8×10^{-2}
250	$4.8v \times 10^{-2}$

Table 5.2: Table with the results of the oscillatory stress simulations for an amplitude of 0.1 Å. ΔW was obtained by calculating the area of the hysteresis loop.

copper samples from [38]. The fractional change in shear modulus $\frac{G_1 - G_2}{G_2}$ was calculated from the simulation between the sample with dislocations and the one with no dislocations, the result is approximately $\frac{1}{2}$. In the case of the samples used in [38], the fractional change in shear modulus gives $\frac{1}{15}$. Note that the sample Cu-Lam of the same reference has dislocation density 1.1×10^{12} cm^{-2}, similar to the one in the simulation. The samples in [38] have dislocations with Burgers vector in many different directions and has dislocations of screw and edge type. Although there is a difference in the fractional change of shear modulus, this is probably related to the differences just mentioned between the samples. The simulation contains dislocations with vector Burgers in the $\langle 110 \rangle$ which is the closest packed plane, that is, the direction in which the direction is the easiest [10]. This direction is the same as the one in which the loading is applied in the simuations.

From the results of the shear modulus we check that the simulations are describing correctly the mechanical properties of copper, and that the stress-strain plots are correct.

Oscillatory shear strain simulations were also done for a lower amplitude of 0.1 Å and temperatures of 0 K, 50 K, 100 K, 1500 K, 200 K and 250 K. The stress-strain plots are shown in figure 5.12. The value of ΔW was calculated for these plots, the results can be found in table 5.2.

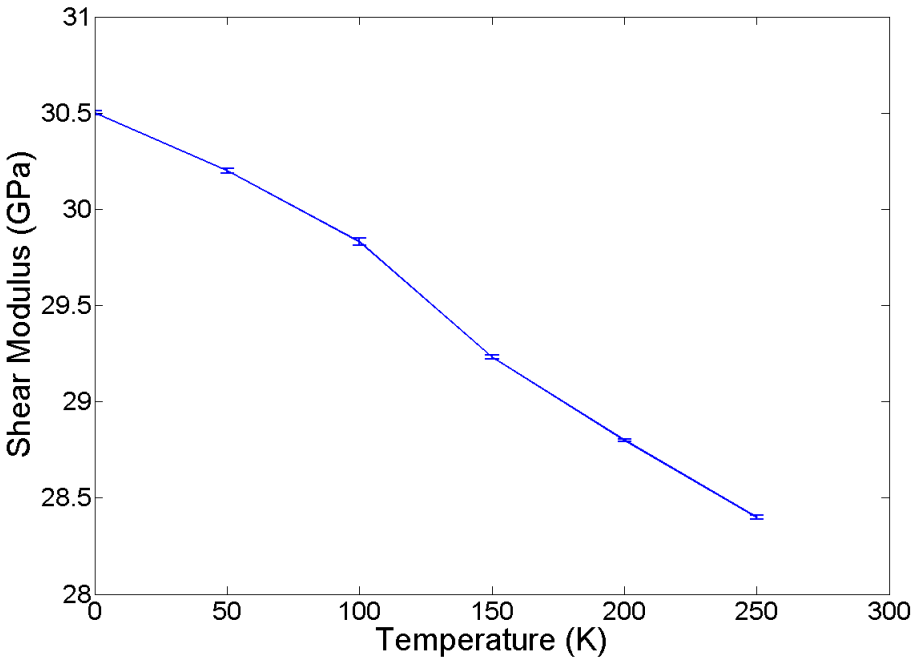

Figure 5.10: Plot of the shear modulus obtained from the stress-strain plots for the sample with dislocations for different temperatures. Compare with plot from [37]. In figure 2 of this reference the shear modulus vs temperature is shown in a copper single crystal, the measured shear modulus for the sample with dislocations is approximately 2.5 times lower because dislocations tend to lower the shear modulus. The slope of the curve in reference [37] is approximately 0.02 Gpa/K, the slope of the curve measured in the samples of this work is approximately 0.01 Gpa/K

5.4.1 Limitations of simulation

Since the simulations were done with molecular dynamics, quantum mechanical effects won't appear in the simulations. One important limitation is the fluctuations of stress, these fluctuations are a limitation to the measurement of the internal friction of the sample. In the previous subsection we calculated the area under the curves ΔW of the stress-strain plots (see table 5.1), but one possibility is that this areas are such because of the fluctuations in the stress. To determine this, the root mean square deviation (RMSD) is calculated in the stress-strain plots. Notice that there are no fluctuations in the strain because this is imposed, and that if there were no fluctuations in the stress and some hysteresis, then the RMSD would be different than zero. Thus, if the fluctuations on the stress-strain plot from a linear function and the fluctuations in the stress as a function of time are of similar size, then the area ΔW comes mainly from the fluctuations, and is not a good measurement of internal friction

The RMSD of the stress as a function of time was measured sampling 64 points of the cycle averaged over 3 cycles, compared to a sine function fitted to the measured stress. The result of these measurements are summarized in table 5.3. Computing RMSD with only 64 points is a limitation when it is considered that the whole cycle has 64000 steps. The root

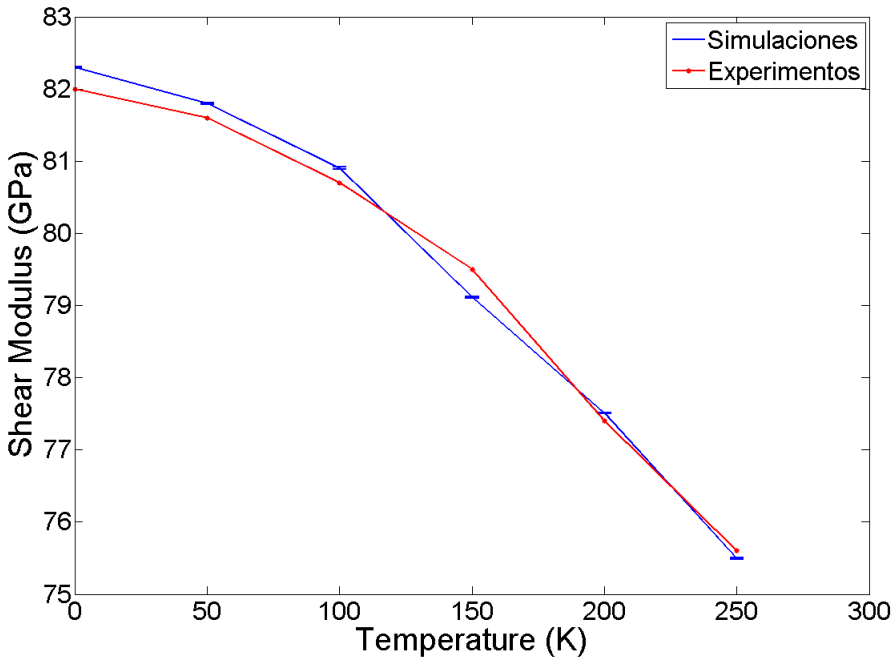

Figure 5.11: Plot of the shear modulus for a copper sample with 1 200 000 atoms and without dislocations for different temperatures. Compare with plot from [37]. In figure 2 of this reference the experimentally measured shear modulus vs temperature is shown in a copper single crystal, the measured shear modulus for the sample without dislocations is very similar for all temperatures. The slope of the curve in reference [37] is approximately 0.02 Gpa/K, the slope of the curve measured in the samples of this work is approximately the same.

mean square deviation for the plots in figure 5.9 were also measured. A straight line was fitted to these graphs, and the RMSD was calculated. The results are summarized in table 5.4. From these two tables we learn that the fluctuations of the stress are the source for the ΔW measured in table 5.1, this is because the size of the stress fluctuations are the same in the stress vs time and stress vs strain plots. Notice that in table 5.3 the fluctuations are similar, either of the same order or bigger than the fluctuations of the stress-strain plots in table 5.4. This means that any possible hysteresis is not being observed because of the fluctuations in the measured stress.

The root mean square deviations for simulations of smaller amplitude were also calculated. Simulations with an amplitude of 0.1 Å were done, in table 5.5 it is shown the RMSD for the stress-time curves obtained, and in 5.6 the RMSD for the stress-strain curve

Finally, the upper bound for uncertainty in stress measurements needed to detect an internal friction of order $Q^{-1} = 10^{-4}$ was calculated. To calculate this we use the result of section 5.3.1 where we obtained through the analytical model that $\Delta W \sim 10^{-2}$ eV. With this result and approximating the hysteresis loop as a parallelogram, it is calculated that the error in the measurement of stress needs to be at most of the order of 10^{-7} eV/ Å^3 or 0.1 Bar. This value was obtained for simulations with a strain amplitude of 0.008. Also we note that these fluctuations come from the presence of the dislocations in the sample. It should be

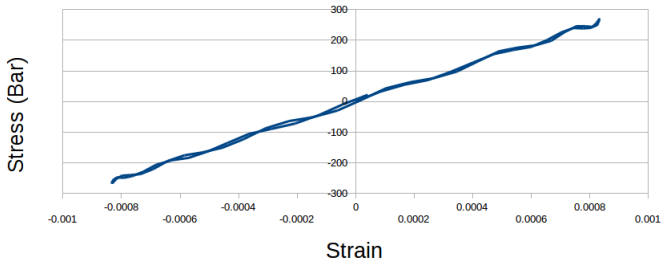

(a) Temperature = 0.0001 K, Amplitude = 0.1 Å

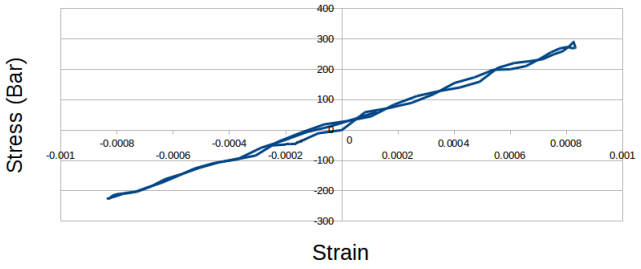

(b) Temperature = 50 K, Amplitude = 0.1 Å

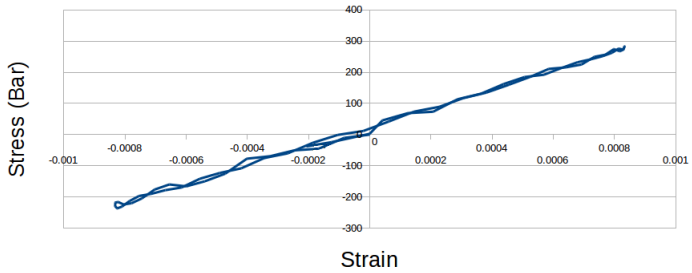

(c) Temperature = 100 K, Amplitude = 0.1 Å

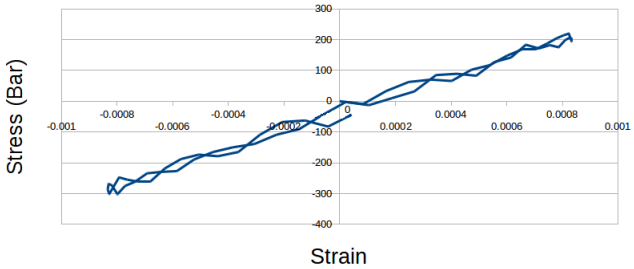

(d) Temperature = 150 K, Amplitude = 0.1 Å

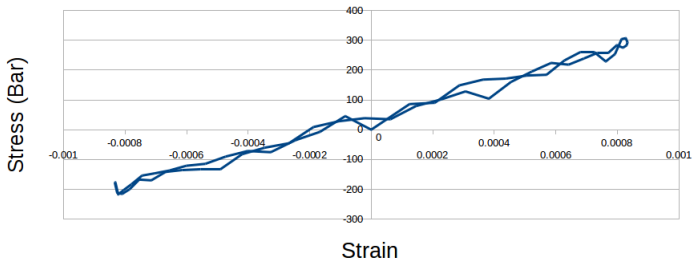

(e) Temperature = 200 K, Amplitude = 0.1 Å

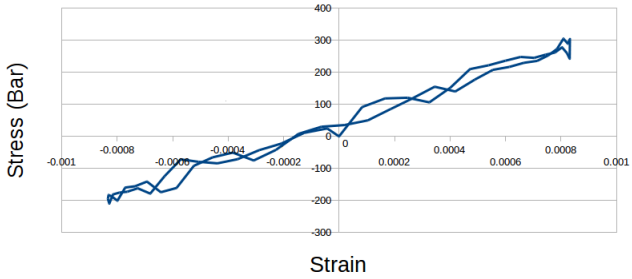

(f) Temperature = 250 K, Amplitude = 0.1 Å

Figure 5.12: Stress vs strain plot. The graph was produced by applying an oscillatory strain on the sample with the period given by (5.11). The amplitude used corresponds to 0.1 Å

Temperature (K)	RMSD Stress (Bar)	RMSD Stress (eV/ Å^3)
0	5.36	3.35×10^{-6}
50	60.16	3.76×10^{-5}
100	30.08	1.88×10^{-5}
150	38.72	2.42×10^{-5}
200	61.12	3.82×10^{-5}
250	46.4	2.9×10^{-5}

Table 5.3: Table with the root mean square deviation (RMSD) of the stress compared to a sine function adjusted to the measured stress in time. The stress is shown in units of Bar and eV/ Å^3. Amplitude of free wall displacement 1 Å and 38 ps.

Temperature (K)	RMSD Stress Bar	RMSD Stress eV/ Å^3
0	5.34	3.34×10^{-6}
50	17.6	1.1×10^{-5}
100	103.84	6.49×10^{-5}
150	20.64	1.29×10^{-5}
200	27.68	1.73×10^{-5}
250	24	1.5×10^{-5}

Table 5.4: Table with the root mean square deviation (RMSD) of the stress compared to a linear function adjusted to the measured stress vs strain. The stress is shown in units of Bar and eV/ Å^3. Amplitude of free wall displacement 1 Å and 38 ps.

Temperature (K)	RMSD Stress (eV/ Å^3)
0	4.28×10^{-6}
50	3.65×10^{-6}
100	4.5×10^{-6}
150	3.5×10^{-6}
200	1.9×10^{-5}
250	2.8×10^{-5}

Table 5.5: Table with the root mean square deviation (RMSD) of the stress compared to a sine function adjusted to the measured stress in time. The stress is shown in units of eV/ Å^3. Amplitude of free wall displacement 0.1 Å and 38 ps.

Temperature (K)	RMSD Stress eV/ Å^3
0	4.27×10^{-6}
50	5.67×10^{-6}
100	7.2×10^{-6}
150	9.42×10^{-6}
200	1.1×10^{-5}
250	1.6×10^{-5}

Table 5.6: Table with the root mean square deviation (RMSD) of the stress compared to a linear function adjusted to the measured stress vs strain. The stress is shown in units of eV/ Å^3. Amplitude of free wall displacement 0.1 Å and 38 ps.

also noted that in simulations for the sample without dislocations, the fluctuations were 100 times smaller than those with dislocations. This is evidence for the fact that the presence itself of the dislocations is the source for the fluctuations.

Conclusion

In this work the behaviour of a copper single crystal with dislocations has been simulated through molecular dynamics. It has been attempted to study the internal friction generated by this sample when subject to oscillatory stress. Once the stress-strain plots were calculated for temperatures from 0 K to 250 K, the area of the hysteresis loops were calculated (the dissipated energy per cycle can be found in table 5.1). Although the Q^{-1} obtained from this simulations is bigger than the corresponding expected Q^{-1} from the analytical model, it is later found that the stress fluctuations are too big to discern the real dissipated energy. Thus, from this work it is possible to calculate an upper bound for the precision required to observe the effect in this type of simulations. Also from the simulations and the calculation of ΔW we deduce that the Peierls Barrier must be very small, since the hysteresis, if present, has not been detected.

It is notable that it is possible to obtain through an analytical model (and parameters obtained through simulations) an order of magnitude for the Q^{-1} that is in agreement with experiments. If this is also true with other FCC models needs to be checked. It was also found that most of the stress fluctuations in the simulations were caused by the movement of the dislocations. During the calculations of the shear modulus of copper without dislocations the fluctuations were a hundred times smaller than the simulations with dislocations, this is reflected in the error of the calculation of the shear modulus. Finally, it is found that it is necessary to lower the stress fluctuations. The upper bound for these fluctuations are of the order of 10^{-7} eV/ Å^3. It may be possible to reduce these fluctuations by averaging the hysteresis curves over many cycles, although this was already done for 3 and 10 cycles which hasn't reduced the fluctuations significantly. This supports the idea that the fluctuations are not white noise, but instead there is a source for theses fluctuations in the interaction between the sound waves and the dislocations.

As future work it would be interesting to lower the stress fluctuations or increasing the internal friction in the samples in order to study this effect. One possibility is creating bigger samples, or including more dislocations, although the computational cost may prove to be prohibitive to get to sufficiently high internal friction. Another option is to study other FCC crystals with higher damping coefficients, this would increase the dissipated energy in the frequency at which the hysteresis is maximum. A third option is to filter the stress time series. By filtering the frequencies of the stress which do not contribute to the formation of the hysteresis it may be possible to observe the dephase between stress and strain.

Bibliography

[1] I. Shin and E. Carter. Possibe origin of the discrepancy in peierls stresses of fcc metas: First-principles simulations of dislocation mobility in aluminium. *Physical Review B*, 88(6):064106, 2013.

[2] J.P. Hirth and J. Lothe. *Theory of Dislocations*. Krieger Publishing Company, second edition, 1982.

[3] F. Marchesoni. Internal friction by pinned dislocations: Theory of the bordoni peak. *Phisical Review Letters*, 74(15):2973–2976, 1995.

[4] A.S. Nowick and B.S. Berry. *Anelastic Relaxation in Crystalline Solids*. Academic Press, first edition, 1972.

[5] M. J. Konstantinovic. Internal friction study of dislocation dynamics in neutron irradiated iron, and iron-copper alloys. *Journal of Nuclear Materials*, 395:75–78, 2009.

[6] M. J. Konstantinovic. Magnetic after-effect study of dislocation relaxation in fe-based alloys. *Journal of Physics D*, 44:305002, 2011.

[7] L.D. Landau and E.M. Lifshitz. *Theory of Elasticity*. Pergamon, third edition, 1986.

[8] R. Peierls. The size of a dislocation. *Proceedings of the Physical Society*, 52(1):34–37, 1940.

[9] F. R. N. Nabarro. Dislocations in a simple cubic lattice. *Proceedings of the Physical Society*, 59(2):256–272, 1947.

[10] D. Hull and D.J. Bacon. *Introduction to Dislocations*. Elsevier, fifth edition, 2011.

[11] J.D. Eshelby. Edge dislocations in anisotropic materials. *Philosophical Magazine*, 40(308):903–912, 1949.

[12] J.D. Eshelby. The interaction of kinks and elastic waves. *Proceedings of the Royal Society*, 266(308):222–246, 1962.

[13] A.H. Cottrell. *Dislocations and Plastic Flow in Crystals*. Oxford University Press, first edition, 1958.

[14] W. Cai, V. Bulatov, J. Chang, J. Li, and S. Yip. Dislocation core effects on mobility. *Philosophical Magazine*, 12(1):1–80, 2004.

[15] P.G. Bordoni, M. Nuovo, and L. Verdini. Relaxation of dislocations in copper. *Il Nuovo Cimento*, 14(2):273–314, 1955.

[16] R. Truell, C. Elbaum, and B.B. Chick. *Ultrasonic Method in Solid State Physics*. Academic Press, first edition, 1969.

[17] D. H. Niblett and J. Wilks. The internal friction of annealed copper at low temperatures. *Proceedings of the Physical Society*, 73(95):95–99, 1959.

[18] A. Seeger. On the theory of the low-temperature internal friction peak observed in metals. *Philosophical Magazine*, 1(7):651–662, 1956.

[19] N.F. Mott and F.R.N. Nabarro. Dislocation theory and transient creep. *Physical Society Bristol Conference Report*, pages 1–19, 1948.

[20] P.G. Bordoni. Elastic and anelastic behavior of some metals at very low temperatures. *Journal of the Acoustical Society of America*, 26(4):495–502, 1954.

[21] F.R. Nabarro. Theoretical and experimental estimates of the peierls stress. *Journal of the Acoustical Society of America*, 75(3):703–711, 1997.

[22] A. Maurel, V. Pagneux, F. Barra, and F. Lund. Interaction between an elastic wave and a single pinned dislocation. *Physical Review B*, 72(17):174110, 2005.

[23] A. Maurel, V. Pagneux, F. Barra, and F. Lund. Wave propagation through a random array of pinned dislocaations: Velocity change and attenuation in a generalized granato and lücke theory. *Physical Review B*, 72(17):174111, 2005.

[24] N. Rodriguez, A. Maurel, V. Pagneux, F. Barra, and F. Lund. Interaction between elastic waves and prismatic dislocation loops. *Journal of Applied Physics*, 106(2):054910, 2009.

[25] J. Marian and A. Caro. Moving dislocations in disordered alloys: Connecting continuum and discrete models with atomistic simulations. *Physical Review B*, 74(2):024113, 2006.

[26] S. A. Skirlo and M. J. Demkowitz. Viscoelasticity of stepped interfaces. *Applied Physics Letter*, 103(17):171908, 2013.

[27] S. Plimton. Fast parallel algorithms for short-range molecular dynamics. *J Comp Phys*, 117(5):1–19, 1995.

[28] A. Stukowski. Visualization and analysis of atomistic simulation data with ovito - the open visualization tool. *Modelling Simul. Mater. Sci. Eng.*, 18(5):012012, 2010.

[29] M.S. Daw and M.I. Baskes. Embedded-atom method: Derivation and application to impurities, surfaces, and other defects. *Physical Review B*, 29(12):6443–6453, 1984.

[30] M.S. Daw, S.M. Foiles, and M.I. Baskes. Embedded-atom method: a review of theory

and applications. *Materials Science Reports*, 9(7-8):251–310, 1993.

[31] Y. Mishin, M. J. Mehl, D. A. Papaconstantopoulos, A. F. Voter, and J. D. Kress. Structural stability and lattice defects in copper: Ab initio, tight-binding, and embedded-atom calculations. *Physical Review B*, 63(22):224106, 2001.

[32] Y. Mishin, D. Farkas, M. J. Mehl, and D. A. Papaconstantopoulos. Interatomic potentials for monoatomic metals from experimental data and ab initio calculations. *Physical Review B*, 59(5):3393–3407, 1999.

[33] C.A. Becker, F. Tavazza, Z. Trautt, and R.A. Buarque de Macedo. Considerations for choosing and using force fields and interatomic potentials in material science and engineering. *Current Opinion in Solid State and Materials Science*, 17(1):277–283, 2013.

[34] A. Granato and K. Lücke. Theory of mechanical damping due to dislocations. *Journal of Applied Physics*, 27(6):583–593, 1956.

[35] A. Granato and K. Lücke. Application of dislocation theory to internal friction phenomena at high frequencies. *Journal of Applied Physics*, 27(7):789–805, 1956.

[36] G.R. Brown and D.H. Nibblet. The bordoni internal friction peak in copper. *Journal of physics D: Applied Physics*, 6(7):809–818, 1973.

[37] W.C. Overton and J. Gaffney. Temperature variation of the elastic constants of cubic elements. i. copper. *Physical Review*, 98(4):969–977, 1955.

[38] C. Espinoza. *Caracterización de densidad de dislocaciones mediante espectroscopía de resonancia ultrasónica no lineal.* Master's thesis, Universidad de Chile, 2013.

Appendices

Appendix A

Time lengths for simulations

In this appendix we summarize in table A.1 the computer time required for the different simulations. For all the simulations 10 nodes of the cluster in the physics department in Universidad de Chile are considered. This cluster has 12 servers with 2 CPU Xeon quad core 5504, each server has 8 cores and there are 96 cores in total. It also has 4 GB of RAM and 250 GB of hard disk space.

The first simulation considered is the equilibration of the sample at 0.0001 K. The high number of steps is needed to avoid big oscillations on the free walls and also to allow oscillations of the dislocations to disappear. The heating of the sample to different temperatures is done for 500000 steps. This process needs to be slow to again avoid violent oscillations from the free walls. The number of steps needed for simulations of constant shear rate will depend on the shear strain applied, this is because the time for the stress to achieve equilibrium will increase with lower shear strains.

Simulation	Computer time (hours)	Number of time steps
Equilibration of sample at 0.0001 K	168	2000000
Heating to 50 K, 100 K, 150 K, 200 K,250 K	40	500000
Thermalization	8	100
Applying constant shear rate	1 to 84	50000 to 1000000
Oscillatory shear strain (1 cycle)	12	189000

Table A.1: Table with the computer time for the different simulations in this work and the number of time steps ($\Delta t = 0.002ps$) in the corresponding simulation.

Appendix B

Partial dislocations in FCC metals

In this appendix a small description of partial dislocations will be given in order to understand the sample used in the dynamical simulations of this thesis where four partial dislocations appear.

The majority of common metals have either a face centered cubic structure (FCC), a body centered cubic structure (BCC) or an hexagonal close packed structure (HCP). The major difference between these structures is the unit cell. These are shown in figure B.1.

Much of the dislocation behaviour in FCC metals is due to the Shockley dissociation [14]. This is a process in which a dislocation with a Burgers vector $\frac{1}{1}\langle 110\rangle$ splits into two partial dislocations (dislocations whose Burgers vector is not a lattice vector). Between both dislocations a stacking fault (SF), i.e. a disordering in the crystallographic planes, is formed. In Miller index notation, the process is written as

$$\frac{1}{2}[110] = \frac{1}{6}[21\bar{1}] + SF + \frac{1}{6}[121].$$

This is a manifestation of the lattice periodicity having an effect on the dislocations that

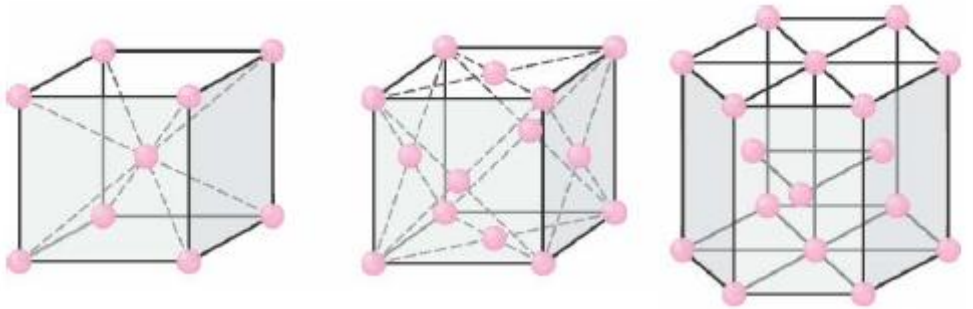

(a) BCC structure (b) FCC structure (c) HCP structure

Figure B.1: Most common crystal structures for metals, body centered cubic (BCC), face centered cubic (FCC) and hexagonal close packed (HCP). In this thesis the focus will be on FCC metals and the core structure of dislocations in this type of structure.

is not predicted by theories in the continuum. The EAM potential used in the simulations describes well the partial dislocation formation. In figure B.2 it is possible to see the partial dislocations in the direction of the dislocation lines and in figure B.3 it is seen in the direction of the normal vector to the slip plane.

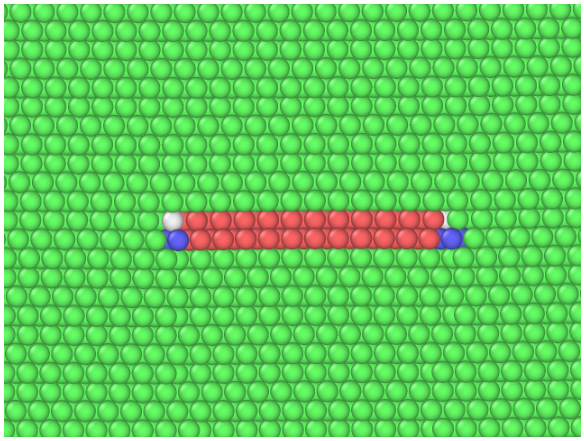

Figure B.2: Dislocation separated in two partial dislocations and a HCP stacking fault seen in the direction of the dislocation line. In green are shown the atoms in a FCC structure, in red HCP, in blue BCC and unknown in gray. The partial dislocation is formed by atoms in BCC and unknown structure.

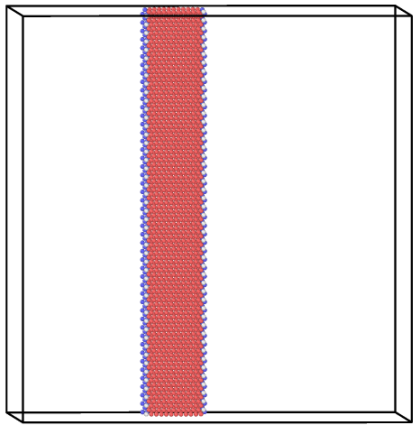

Figure B.3: Dislocation separated in two partial dislocations and a HCP stacking fault seen in the direction of the normal vector to the slip plane. In red are the atoms in HCP structure, in blue BCC and unknown in gray. The partial dislocation is formed by atoms in BCC and unknown structure.

The Shockley dissociation is energetically favourable in FCC metals. To see this we must compare:

- The energy given by the presence of a $\frac{1}{2}\langle 110\rangle$ dislocation to the energy given by the presence of the corresponding partial dislocations. From this we will deduce that there is a net energy reduction from dissociation.
- The presence of the stacking fault and the interaction of the partial dislocations with each other. From this we will deduce that there is an equilibrium distance given by the competition of these two energies

First note that the energy due to the presence of the dislocation is Gb^2 where G is the shear modulus and b is the Burgers vector [10]. The energy of the perfect dislocation is

$$G(\frac{a}{2}\langle 110\rangle)^2 = \frac{Ga^2}{2}$$

where a is the lattice vector. The energy of the two partial dislocations is

$$2G(\frac{a}{6}\langle 112\rangle)^2 = \frac{Ga^2}{3}$$

Thus there is an energy reduction of $\frac{Ga^2}{6}$ by just considering the energy due to the presence of the dislocations.

Now we show that the two generated partial dislocations have an equilibrium distance. For this, we must consider the force of the interaction between the two partial dislocations and the force of the interaction between the stacking fault and each partial dislocation.

The force of the interaction between the partial dislocations will be large at short distances. The dislocations repel each other because of the directions taken by the Burgers vector and the force has a 1/d dependence on the distance d between the dislocations [10]. Then because of this interaction the partial dislocations will tend to maximize d.

The energy of the stacking fault generated between the partial dislocations is proportional to the area covered by the stacking fault [10]. If we consider this energy per unit length as we do for the dislocation then this energy is proportional to the distance d between the partial dislocations. This energy will provide a constant force per unit length line that tends to pull the dislocations together [10]. The effect is that the partial dislocations will tend to minimize d because of their interaction with the stacking fault.

In total we have a force with a 1/d dependence and a constant force in the opposite direction. The net result is an equilibrium distance between the partial dislocations. This can be seen in the samples of the atomistic simulations, for example in figure 5.1.